INFORMATION TO USERS

This manuscript has been reproduced from the microfilm master. UMI films the text directly from the original or copy submitted. Thus, some thesis and dissertation copies are in typewriter face, while others may be from any type of computer printer.

The quality of this reproduction is dependent upon the quality of the copy submitted. Broken or indistinct print, colored or poor quality illustrations and photographs, print bleedthrough, substandard margins, and improper alignment can adversely affect reproduction.

In the unlikely event that the author did not send UMI a complete manuscript and there are missing pages, these will be noted. Also, if unauthorized copyright material had to be removed, a note will indicate the deletion.

Oversize materials (e.g., maps, drawings, charts) are reproduced by sectioning the original, beginning at the upper left-hand corner and continuing from left to right in equal sections with small overlaps.

Photographs included in the original manuscript have been reproduced xerographically in this copy. Higher quality 6" x 9" black and white photographic prints are available for any photographs or illustrations appearing in this copy for an additional charge. Contact UMI directly to order.

ProQuest Information and Learning
300 North Zeeb Road, Ann Arbor, MI 48106-1346 USA
800-521-0600

UMI®

Studies in Low Dimensions:

Modulated Stripe Phase

in the Quantum Hall Effect;

Correlators in the Calogero-Sutherland Model.

by Lenny Tevlin

A dissertation submitted to the Graduate Faculty in Physics

in partial fulfillment of the requirements for the degree of

Doctor of Philosophy, The City University of New York.

2002

ProQuest information and Learning Company
300 North Zeeb Road
P.O. Box 1346
Ann Arbor, MI 48106-1346

This manuscript has been read and accepted for the Graduate Faculty in Physics in satisfaction of the dissertation requirement for the degree of Doctor of Philosophy.

1/28/02
Date

Prof. Joseph L. Birman, City College
Chair of Examining Committee

Jan 31, 2002
Date

Prof. Louis S. Celenza, Brooklyn College
Executive Officer

Prof. Joel I. Gersten, City College

Prof. V. Parameswaran Nair, City College

Prof. Jerome K. Percus, New York University

Prof. Carl M. Shakin, Brooklyn College

Meir Weger
Prof. Meir Weger, Hebrew University

Supervisory Committee

THE CITY UNIVERSITY OF NEW YORK

Abstract.

Studies in Low Dimensions:

Modulated Stripe Phase in the Quantum Hall Effect;

Correlators in the Calogero-Sutherland Model.

by Lenny Tevlin

Advisor: Prof. Joseph L. Birman

In the first part of this work I investigate the structure of the ground state of a two-dimensional electron gas in the presence of weak transverse magnetic field and a weak external periodic potential. The ground state of the system without periodic potential is thought to be a unidirectional guiding center charge density wave. This state describes electrons arranged in stripes periodic in one direction (the stripes are uniform in the other direction); therefore this state often referred to as a stripe state.

The effect of the periodic potential is considered in two cases: when the potential is perpendicular to the direction of the stripes. and when it is parallel to them. In both cases we calculate the cohesive energy. In the first case we also obtain modifications of positions and widths of the

stripes due to the external potential. In the second case the stripes can only change their widths and we calculate this change. I also study the conductivity of the striped state in the periodic potential. I find that the correction to the conductivity scales as the square root of the amplitude of the applied potential when the potential is perpendicular to the stripes. The sign of the correction depends on the value of the ratio of the period of the external potential and the natural period of the charge density wave. Certain period matching conditions lead to a decrease, while others to an increase in the conductivity.

In the second part, I present the calculation of correlations functions of the Calogero-Sutherland model. The model, describing one-dimensional electrons with long-ranged interactions confined to a circle, is exactly solvable. I extend the method of Jack polynomials to the calculation of the dynamical polarization tensor.

Contents

List of Figures

Chapter 1

Preface.

I used to be indecisive but now I am not so sure.

attributed to **Boscoe Pertwee**[1]. *18th century wit.*

[1] as quoted in [64].

1.1 Overview of Results Concerning Two Dimensional Electrons in a Weak Magnetic Field.

One fundamental goal of contemporary condensed matter physics seems to be to understand the ground state of the two-dimensional electron system and to explore its experimental signatures. In the presence of a large perpendicular magnetic field B, the kinetic energy of two-dimensional electrons becomes quantized into discrete highly degenerate Landau levels. At high B only the lowest ($N = 0$) Landau level is occupied, and the two-dimensional electron system exhibits its most spectacular phenomenon: the Fractional Quantized Hall effect [71]. At lower magnetic fields the higher Landau levels become occupied, and in the third or higher ($N \geq 2$) Landau levels no Fractional Quantum Hall states have been observed. Recent experiments have nevertheless uncovered extraordinary transport signatures unique to the high Landau level regime, pointing to the existence of a new class of many-body states distinct from the incompressible quantum fluids responsible for the Fractional Hall states [8, 10]. The most striking of these signatures is the development, at very low temperatures, of strong anisotropies in the longitudinal resistance of the two-dimensional electron system. Some details of the experimental results are reviewed in Sec. 3.1.

This experimental discovery was anticipated theoretically by Fogler *et. al* [11] and Moessner and Chalker [13] who proposed the guiding center charge density wave states as the ground state in partially filled higher Landau levels [8], [10] The observations of anisotropic conducting states between filling fractions ν of 9/2 and 21/2 is now considered to be convincing experimental evidence for the existence of these striped states at these filling fractions. Exact diagonalization studies [17] on small systems have given further support to the existence of a unidirectional charge density wave ground state (also referred to as a stripe state) in a partially filled Landau level. The theory of the formation of the stripe state is discussed in Sec. 3.2 and Sec. 3.6.1.

The renormalization group analysis of Macdonald and Fisher [16] suggested that the stripe state is unstable against the formation of a Wigner crystal due to backscattering. Numerical calculations of Côté and Fertig [18] indicate that this highly anisotropic crystal is indistinguishable from the unidirectional charge density wave. Hartree-Fock approximation therefore seems to adequately describe the ground state of the partially filled higher Landau levels. Lopatnikova *et. al* [19] have described the low energy excitations of the stripe state and calculated the low energy elastic parameters of the system.

It seems natural to study the interplay of interaction-induced periodicity with an external commensurable (or incommensurable) periodic potential. Indeed mea-

surements of the magnetoresistance in lateral superlattices with period close to the expected period of the charge density wave have been performed [23]. These experiments show a shallow and broad minimum with peaks on both sides when the direction of the current is parallel to the direction of the external potential and a small peak when the direction of the current is perpendicular to the potential. On the theoretical side, numerical works [27], [25] have initiated the study of the influence of the periodic perturbation. By applying an added periodic potential we put an additional externally controlled length scale into the problem. Thereby we can test the robustness of the previous solutions, and predict new physical effects.

In this part of the thesis I investigate the structure of the ground state of two-dimensional electrons in a weak magnetic field at half filling in the presence of a weak periodic potential. The goal is to determine the circumstances when each orientation of the stripes with respect to the external modulation (see below) is realized, and establish possible experimental signatures of a given orientation. The analogous problem for the Fractional Quantum Hall states has been considered in [20] and [21].

One can distinguish two cases: when the external modulation is perpendicular to the direction of the stripes in sec. 4.2, and when it is parallel to them in sec. 4.3.

When the external modulation is perpendicular to the direction of the stripes, each stripe can expand or shrink as well as move as a whole with respect to its unperturbed

position to take advantage of the external potential and lower its energy. Whereas when the external modulation is parallel to the stripes, each stripe can reduce its energy by modulating its density along the applied potential and changing its width (without shifting its center).

In both cases I calculate the cohesive energy and find a decrease in the cohesive energy proportional to the square of the amplitude in agreement with numerical simulations [27], [25].

Based on the comparison of the cohesive energies, in Sec. (4.4), I calculate that alignment parallel to the direction of the external modulation has lower cohesive energy for all periods of the external potential.

In the first case I also obtain modifications of positions and widths of the stripes due to the external potential (see section 4.2). In the second case the stripes can only change their widths and I calculate this change.

I also study the conductivity of the striped state in the periodic potential. I find that the correction to the conductivity scales as the square root of the amplitude of the applied potential when the modulation is perpendicular to the stripes. The sign of the correction depends on the value of the ratio of the period of the external potential and the natural period of the CDW. Certain period matching conditions lead to a decrease , while others to an increase, in the conductivity (see section 4.5).

1.2 Overview of Results Concerning Correlation Functions of the Calogero-Sutherland Model.

Besides being intrinsically interesting as models describing artificially made one-dimensional systems, exactly solvable models of electrons restricted to one dimension can be thought of as a proving ground for the emerging methods of dealing with strongly interacting particles.

In the world of one-dimensional models a special place is reserved for the Calogero-Sutherland Model. The introduction of this model dates back to Moser [31] for classical systems and Calogero and Sutherland [32] for quantum systems.

The Calogero-Sutherland model is intimately related to the circular ensembles in random matrix theory. In particular, the eigenvalue distribution function for the orthogonal, unitary, and symplectic random matrices correspond to the ground state wavefunctions of the Calogero-Sutherland model at specific values of the interaction. First static correlation functions of the Calogero-Sutherland model have been calculated using the techniques developed for the random matrices [73].

Later, Simons *et. al.* [34] succeeded in utilizing the supersummetric algebra approach to the calculation of the dynamical density-density correlation function for the Calogero-Sutherland model at special values of the coupling constant. Haldane and

Zirnbauer [45] used a similar method to calculate the one-particle retarded Green's function in the symplectic case.

The most powerful approach was developed by Z. Ha [40], who recognized that the eigenstates of the Calogero-Sutherland model can be written in terms of Jack polynomials [59, 58]. This allowed him to calculate the exact dynamical density-density correlation function and the one-particle retarded Green's function at arbitrary interaction strength. Further progress was made by F. Lesage *et. al.*, who calculated the advanced Green's function at arbitrary interaction strength.

In this part of the work I will extend these methods to the calculation of the full dynamical polarization tensor.

Acknowledgements.

I am deeply grateful to my advisor, Professor Joseph L. Birman, for his patient guidance and encouragement throughout the years of our relationship.

I would also like to thank Ilya Vekhter for his friendship and numerous illuminating discussions.

Part I

Two Dimensional Electrons in a Magnetic Field and Periodic Potential.

Glossary.

For convenience. below I have collected definitions and typical values of parameters used in Part I of this work.

They are based on the parameters of the system. such as the effective electron mass in GaAs

$$m = 0.068 m_e.$$

magnetic field B (taken to be 2 T for estimates). density

$$n \sim 2.7 \times 10^{11} cm^{-2}$$

or Fermi wavevector in zero magnetic field

$$k_F = \sqrt{2\pi n}.$$

background dielectric constant

$$\kappa \sim 13$$

And fundamental constants: electric charge e, electron mass m_e, Plank's constant $\hbar$, speed of light c.

Definition	**Symbol**	**Typical value**
Cyclotron energy:	$\hbar\omega_c \equiv \hbar\frac{eB}{mc}$	4 meV
Magnetic length:	$\ell \equiv \sqrt{\frac{\hbar c}{eB}}$	15 nm
Cyclotron radius:	$R_c \equiv \sqrt{2N+1}\,\ell$	
Effective Bohr radius:	$a_B \equiv \frac{\hbar^2\kappa}{me^2}$	10 nm
Filling factor:	$\nu \equiv k_F^2\ell^2$	$\frac{9}{2}, \frac{11}{2}, \frac{13}{2}$
Landau Level index:	N	≥ 2
Average filling factor of the partially filled Landau level:	$\bar{\nu} = \nu - 2N$	$\frac{1}{2}$
The parameter characterizing the strength of electron-electron interactions:	$r_s \equiv (\pi n a_B^2)^{-1/2} = \frac{\sqrt{2}}{k_F a_B}$	~ 0.9
The electron density of a filled Landau level:	$n_L = \frac{1}{2\pi\ell^2}$	
Form-factor:	$F(q) = \exp\left(-\frac{q^2\ell^2}{4}\right) L_N\left(\frac{q^2\ell^2}{2}\right)$	
The strength of Hartree-Fock interaction:	$u_0 = \hbar\omega_c/2\pi^2 R_c$	

Chapter 2

One Particle Properties of Electrons in a Magnetic Field and Periodic Potential.

2.1 One particle properties.

To a certain extent, the structure of (interacting) many-particle state(s) we are interested in is a reflection of one-particle (noninteracting) properties: the particle trajectory (in classical case) and its wavefunction (in quantum mechanical). It is the ring-like structure of electronic wave-functions on higher Landau levels that is responsible for the creation of charge density wave state that will be the focus of subsequent chapters.

I will examine one particle dynamics both from the classical in Sec. 2.1.1 and quantum mechanical points of view in Sec. 2.1.2. As I am ultimately interested in the combined effect of the interactions and external periodic potential, I will look at the influence of the periodic potential on one-particle properties in Sec. 2.2.

2.1.1 Classical Mechanics of a Particle in a Magnetic Field in Two Dimensions.

The classical Lagrangian for a particle in a constant magnetic field is [67]:

$$\mathcal{L} = \frac{1}{2} m \dot{x}^\mu \dot{x}^\mu - \frac{e}{c} \dot{x}^\mu A^\mu. \tag{2.1}$$

where $\mu = 1, 2$ refers to x and y respectively and $\mathbf{A}$ is the vector potential evaluated at the position of the particle. (I will use the repeated index summation convention.)

Using

$$\frac{\delta \mathcal{L}}{\delta x^\nu} = -\frac{e}{c}\dot{x}^\mu \, \partial_\nu A^\mu \tag{2.2}$$

and

$$\frac{\delta \mathcal{L}}{\delta \dot{x}^\nu} = m\dot{x}^\nu - \frac{e}{c}A^\nu \tag{2.3}$$

the Euler-Lagrange equation of motion becomes

$$m\ddot{x}^\nu = -\frac{e}{c}\left[\partial_\nu A^\mu - \partial_\mu A^\nu\right]\dot{x}^\mu. \tag{2.4}$$

Using

$$\mathbf{B} = \nabla \times \mathbf{A} \tag{2.5}$$

the equations of motion can be explicitly written

$$\begin{aligned} m\ddot{x} &= -\frac{eB}{c}\dot{y} \\ m\ddot{y} &= -\frac{eB}{c}\dot{x}. \end{aligned} \tag{2.6}$$

The general solution of these equations corresponds to motion in a circle (or cycloid in three dimensions) of arbitrary radius R

$$\mathbf{r} = \left(x_0 + R\cos(\omega_c t + \delta),\, y_0 + R\sin(\omega_c t + \delta)\right). \tag{2.7}$$

Here $\mathbf{r_0} = (x_0, y_0)$ is the position of the center of the orbit, δ is an arbitrary initial phase, and

$$\omega_c \equiv \frac{eB}{mc} \tag{2.8}$$

is the classical cyclotron frequency. The period of the orbit is independent of the radius and the tangential velocity $\mathbf{v} = (-\omega_c R \sin(\omega_c t + \delta), \omega_c R \cos(\omega_c t + \delta))$ controls the radius:

$$R = \frac{v}{\omega_c} \tag{2.9}$$

A fast particle travels in a large circle but returns to the starting point in the same interval of time as a slow particle which (necessarily) travels in a small circle. On the classical level the problem possesses an invariant (angular momentum):

$$\Lambda_z = m\mathbf{r} \times \mathbf{v} \cdot \hat{z} - \frac{eB}{2c}(\mathbf{r} \times \hat{z})^2. \tag{2.10}$$

It is a simple matter to verify that $\{H, \Lambda_z\} = 0$, due to rotational symmetry, where $\{,\}$ are the Poisson brackets.

In preparation for the quantum mechanical treatment I now turn to the Hamiltonian formulation [66]. Since we have the Lagrangian we can deduce the canonical momentum

$$\begin{aligned} p^\mu &\equiv \frac{\delta \mathcal{L}}{\delta \dot{x}^\mu} \\ &= m\dot{x}^\mu - \frac{e}{c}A^\mu. \end{aligned} \tag{2.11}$$

and the Hamiltonian

$$\begin{aligned} H[\mathbf{p}, \mathbf{x}] &\equiv \dot{x}^\mu p^\mu - \mathcal{L}(\dot{\mathbf{x}}, \mathbf{x}) \\ &= \frac{1}{2m}\left(p^\mu + \frac{e}{c}A^\mu\right)\left(p^\mu + \frac{e}{c}A^\mu\right). \end{aligned} \tag{2.12}$$

The quantity

$$\Pi^\mu \equiv p^\mu + \frac{e}{c}A^\mu \tag{2.13}$$

is the mechanical momentum. Hamilton's equations of motion

$$\dot{x}^\mu = \frac{\partial H}{\partial p^\mu} = \frac{1}{m}\Pi^\mu \tag{2.14}$$

$$\dot{p}^\mu = -\frac{\partial H}{\partial x^\mu} = -\frac{e}{mc}\left(p^\nu - \frac{e}{c}A^\nu\right)\partial_\mu A^\nu \tag{2.15}$$

show that it is the mechanical momentum, not the canonical momentum, which is equal to the usual expression related to the velocity

$$\Pi^\mu = m\dot{x}^\mu. \tag{2.16}$$

Using Hamilton's equations of motion we can recover Newton's law for the Lorentz force given by (2.6).

To write down the Poisson brackets of the invariant Λ_z with the mechanical momentum and position more economically, I introduce

$$\Pi_\pm = \Pi_x \pm i\Pi_y \text{ and } \zeta_\pm = x \pm iy \tag{2.17}$$

Then the complete algebra of Poisson brackets is:

$$\{H, \Lambda_z\} = 0$$

$$\{H, \Pi_\pm\} = \pm\Pi_\pm$$

$$\begin{aligned} \{H, \zeta_\pm\} &= \pm\zeta_\pm \\ \{\Lambda_\pm, \Pi_\pm\} &= \pm\Pi_\pm \\ \{\Lambda_\pm, \zeta_\pm\} &= \pm\zeta_\pm \end{aligned} \tag{2.18}$$

I will show below that upon quantization this algebraic structure is preserved with Poisson brackets replaced by Lie brackets.

It is interesting to notice that it is possible for the particle to have a finite velocity while having zero (canonical) momentum. Furthermore the canonical momentum is dependent on the choice of gauge for the vector potential and therefore is not a physical observable. The mechanical momentum, being simply related to the velocity (and hence the current) is physically observable and gauge invariant. The classical equations of motion only involve the curl of the vector potential and so the particular gauge choice is not important at the classical level.

2.1.2 Quantum Mechanical Properties of a Particle in a Magnetic Field in Two Dimensions.

The quantum mechanical Hamiltonian for a spinless electron in the magnetic field is [68]:

$$\hat{H} = \frac{1}{2m}\left(\mathbf{p} - \frac{e}{c}\mathbf{A}\right)^2. \tag{2.19}$$

where **p** and **A** are now quantum mechanical operators. The quantum mechanical analogs of the classical quantities x_0, y_0, r_0^2, R^2 are

$$\begin{aligned}
\hat{x}_0 &= \hat{x} - \frac{\hat{v}_y}{\omega_c} = \hat{x} - \frac{1}{m\omega_c}(-i\hbar\frac{\partial}{\partial y} - \frac{e}{c}A_y) \\
\hat{y}_0 &= \hat{y} + \frac{\hat{v}_x}{\omega_c} = \hat{y} - \frac{1}{m\omega_c}(-i\hbar\frac{\partial}{\partial x} - \frac{e}{c}A_x) \\
\hat{r}_0^2 &= \hat{x}_0^2 + \hat{y}_0^2 \\
\hat{R}^2 &= \frac{\hat{v}_x^2 + \hat{v}_y^2}{\omega_c^2}.
\end{aligned}$$

where $\hat{v}_\mu = \frac{i}{m\hbar}[\hat{H}, \hat{r}_\mu] = \frac{1}{m}(-i\hbar\frac{\partial}{\partial r_\mu} - \frac{e}{c}A_\mu)$. The commutators of the velocity components read:

$$[\hat{v}_x, \hat{v}_y] = i\frac{\hbar^2}{m^2\ell^2}. \tag{2.20}$$

where I have introduced the magnetic length

$$\ell = \sqrt{\frac{\hbar c}{eB}} \tag{2.21}$$

One can easily establish that

$$[\hat{H}, \hat{x}_0] = [\hat{H}, \hat{y}_0] = [\hat{H}, \hat{R}^2] = 0 \tag{2.22}$$

but

$$[\hat{x}_0, \hat{y}_0] = -i\ell^2 \tag{2.23}$$

In fact, we can see that the operator corresponding to the radius of the cyclotron orbit is proportional to the Hamiltonian, $\hat{R}^2 = \frac{2\hat{H}}{m\omega}$, and therefore will have well defined eigenvalues for every eigenstate. The noncommutativity of $\hat{x}_0$ and $\hat{y}_0$ implies that the center of the orbit obeys the uncertainty relation $\Delta\hat{x}_0\Delta\hat{y}_0 \geq \ell^2/2$. However, the position of the square of the center of the orbit is conserved: $[\hat{H}, \hat{r}_0^2] = [\hat{R}^2, \hat{r}_0^2] = 0$. (The operator $\hat{r}_0^2$ is a linear combination of the Hamiltonian and the angular momentum operator $\hat{\Lambda}_z$.) The coordinates of the center of the orbit become commutative in the infinite field limit where $\ell \to 0$.

The algebraic structure of the Hamiltonian (2.19) becomes clear with the introduction of the operator analogs of (2.17):

$$\hat{\Pi}_\pm = \hat{\Pi}_x \pm i\hat{\Pi}_y \text{ and } \zeta_\pm = x \pm iy \tag{2.24}$$

and the angular momentum operator Λ_z:

$$\hat{\Lambda}_z = -i\mathbf{r} \times \nabla \cdot \hat{z} + \frac{e}{2c}(\mathbf{r} \times \hat{z})^2 B. \tag{2.25}$$

Then the Hamiltonian can be expressed as

$$\hat{H} = \frac{1}{2}(\hat{\Pi}_+\hat{\Pi}_- - \hat{\Pi}_-\hat{\Pi}_+) \tag{2.26}$$

and the algebra of $\hat{H}, \hat{\Lambda}_z, \hat{\Pi}_\pm$ is:

$$[\hat{H}, \hat{\Lambda}_z] \quad = 0$$

$$[\hat{H}, \hat{\Pi}_\pm] = \pm\hat{\Pi}_\pm$$
$$[\hat{\Lambda}_z, \hat{\Pi}_\pm] = \pm\hat{\Pi}_\pm \tag{2.27}$$

Expressed in the algebraic language, these commutation relations imply that $\hat{\Pi}_\pm, \hat{\Lambda}_z$ constitute an $SU(2)$ Lie algebra, while the Hamiltonian is the bilinear quadratic Casimir operator of this algebra (and belongs to the enveloping algebra of $SU(2)$).

To display the wavefunctions one has to choose a gauge for the vector potential. One popular and convenient choice is the Landau gauge:

$$\mathbf{A}(\mathbf{r}) = xB\hat{y} \tag{2.28}$$

which obeys $\nabla \times \mathbf{A} = B\hat{z}$. In this gauge the vector potential points in the y direction but varies only with the x position, as illustrated in Fig. (2.1). Hence the system still has translation invariance in the y direction. The magnetic field (and hence all the physics) is translationally invariant, while the Hamiltonian is not. The Hamiltonian can be written in the Landau gauge as

$$H = \frac{1}{2m}\left(p_x^2 + (p_y + \frac{e}{c}Bx)^2\right) \tag{2.29}$$

Taking advantage of the translation symmetry in the y direction, a separation of variables can be accomplished by writing the wave function in the form

$$\psi_k(x, y) = e^{iky} f_k(x). \tag{2.30}$$

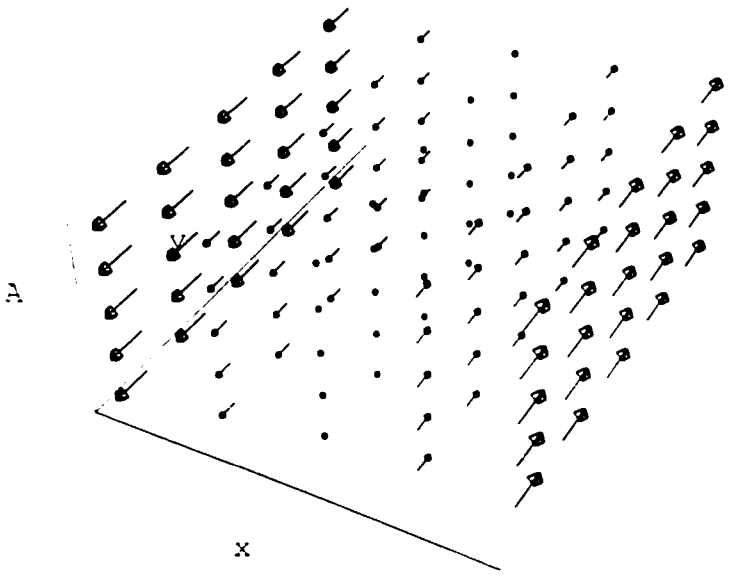

Figure 2.1: Illustration of the Landau gauge vector potential $\mathbf{A} = xB\hat{y}$. The magnetic field is perfectly uniform, but the vector potential has a preferred origin and orientation corresponding to the particular gauge choice.

This has the advantage that it is an eigenstate of p_y and hence one can make the replacement $p_y \longrightarrow \hbar k$ in the Hamiltonian. After separating variables one has the effective one-dimensional Schrödinger equation

$$H_k f_k(x) = \epsilon_k f_k(x). \tag{2.31}$$

where

$$H_k \equiv \frac{1}{2m} p_x^2 + \frac{1}{2m}\left(\hbar k + \frac{eB}{c} x\right)^2. \tag{2.32}$$

This is simply a one-dimensional displaced harmonic oscillator [1]:

$$H_k = \frac{1}{2m}p_x^2 + \frac{1}{2}m\omega_c^2\left(x + k\ell^2\right)^2 \tag{2.33}$$

whose frequency is the classical cyclotron frequency and whose central position $X = -k\ell^2$ is determined by the y momentum quantum number. Thus for each plane wave chosen for the y direction there will be an entire family of energy eigenvalues

$$\epsilon_{kN} = (N + \frac{1}{2})\hbar\omega_c \tag{2.34}$$

which depend only on N and are completely independent of the y momentum $\hbar k$. The corresponding eigenfunctions are:

$$\Psi_{k,N}(x,y) = \frac{e^{iyX/\ell^2}}{\pi^{1/4}\sqrt{2^N N!\ell L_y}}\exp\left[-\frac{(x-X)^2}{2\ell^2}\right]H_N\left(\frac{x-X}{\ell}\right) \tag{2.35}$$

Here L_y is the y dimension of the system. $H_N(x)$ is (as usual for harmonic oscillators) the N^{th} Hermite polynomial [74] displaced to the new central position X. ℓ is the magnetic length as introduced in (2.21) The position X is called a "guiding center coordinate". The wavefunctions are extended in the $\hat{y}$ direction and have a finite spread in the $\hat{x}$ direction.

These harmonic oscillator levels, labelled by N are called Landau levels. The cyclotron radius takes discrete values proportional to the square root of the Landau level index:

$$R_c^2 = (2N + 1)\ell^2 \tag{2.36}$$

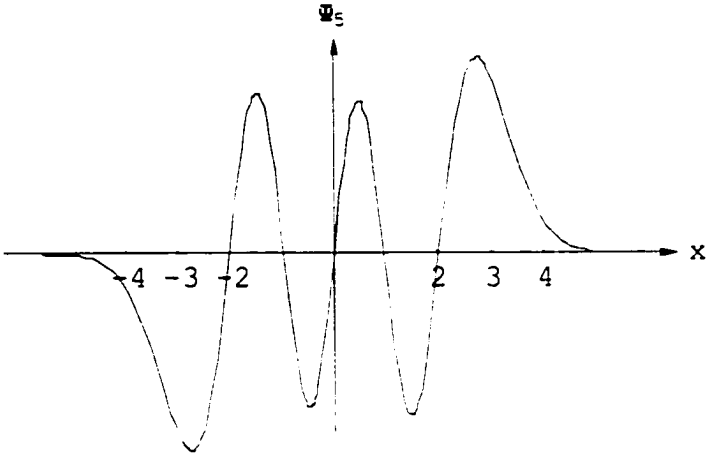

Figure 2.2: Illustration of the x dependance of the one particle wavefunction in the fifth Landau level. The wavefunction decays very rapidly for x greater than the cyclotron radius $R_c = \sqrt{11} \approx 3.3$.

The cyclotron radius determines the spread of the wavefunction in the x direction. These wavefunctions are also eigenfunctions of the operator x_0 with the eigenvalue $-\hbar k/m\omega$. A graph of $\Psi_{0,5}$ is shown on the Figure 2.2.

Due to the lack of dependence of the energy on k, the degeneracy of each level is enormous, as I will now show assuming periodic boundary conditions in the y direction. This implies that $X = \frac{2\pi\ell^2}{L_y}s$, with s integer. Because of the vector potential, it is impossible to simultaneously have periodic boundary conditions in the x direction. However since the basis wave functions are harmonic oscillator polynomials multiplied by strongly converging gaussians, they rapidly vanish for positions away from the

center position $X = -k\ell^2$. Let us suppose that the sample is rectangular with dimensions L_x, L_y and that the left hand edge is at $x = -L_x$ and the right hand edge is at $x = 0$. Then the values of the wavevector k for which the basis state is substantially inside the sample run from $k = 0$ to $k = L_x/\ell^2$. It is clear that the states at the left edge and the right edge differ strongly in their k values and hence periodic boundary conditions are impossible. (The best one can achieve is so-called quasi-periodic boundary conditions in which the phase difference between the left and right edges is zero at the bottom and rises linearly with height, reaching $2\pi N_\Phi \equiv L_x L_y/\ell^2$ at the top. The eigenfunctions with these boundary conditions are Jacobi elliptic theta functions [74] which are linear combinations of the gaussians discussed here [70].) The total number of states in each Landau level is then

$$\frac{L_y}{2\pi}\int_0^{L_x/\ell^2} dk = \frac{L_x L_y}{2\pi\ell^2} = N_\Phi \tag{2.37}$$

where

$$N_\Phi \equiv \frac{BL_xL_y}{\Phi_0} \tag{2.38}$$

is the number of flux quanta penetrating the sample. Here $\Phi_0 \equiv hc/e$ is the magnetic flux quantum. Thus there is one state per Landau level per flux quantum.

Even though the family of allowed wavevectors is only one-dimensional, we find that the degeneracy of each Landau level is extensive in the two-dimensional area. The reason for this is that the spacing between wave vectors allowed by the periodic

boundary conditions $\frac{2\pi}{L_y}$ decreases while the range of allowed wave vectors $[0, L_x/\ell^2]$ increases with increasing L. One may also worry that for very large samples, the range of allowed values of k will be so large that it will fall outside the first Brillouin zone forcing us to include band mixing and the periodic lattice potential beyond the effective mass approximation. This is not true however, since the canonical momentum is a gauge dependent quantity. The value of k in any particular region of the sample can be made small by shifting the origin of the coordinate system to that region (thereby making a gauge transformation).

The width of the harmonic oscillator wave functions in the N^{th} Landau level is of order of the cyclotron radius, $\sqrt{N}\ell$. This is microscopic compared to the system size, but the spacing between the centers

$$a = \frac{2\pi\ell^2}{L_y} \tag{2.39}$$

is vastly smaller (assuming $L_y \gg \ell$). Thus the supports of the different basis states are strongly overlapping (but they are still orthogonal).

It is often convenient, in particular for the physics in the lowest Landau level, to analyze the problem in the symmetric gauge

$$\mathbf{A} = \frac{1}{2}\mathbf{B} \times \mathbf{r} \tag{2.40}$$

Unlike the Landau gauge which preserves translation symmetry in one direction,

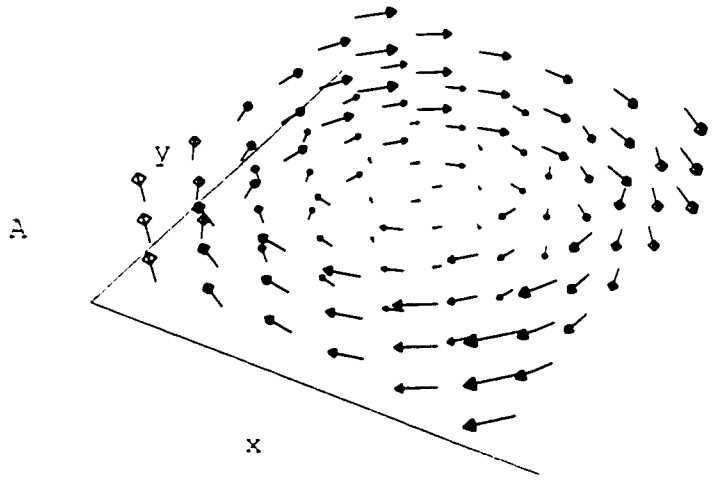

Figure 2.3: Illustration of the symmetric gauge vector potential $\mathbf{A} = \frac{1}{2}B(yx - xy)$. The vector potential is rotationally symmetric around the origin.

the symmetric gauge preserves rotational symmetry about the origin. Hence we anticipate that angular momentum (rather than y linear momentum) will be a good quantum number in this gauge. Indeed the ring-like structure of the higher Landau level wavefunctions becomes manifest in the symmetric gauge.

For simplicity I will restrict myself to the lowest Landau level only and (simply to avoid some awkward minus signs) change the sign of the B field: $\mathbf{B} = -B\hat{z}$. With these restrictions, it is not hard to show that the solutions of the free-particle Schrödinger equation in the lowest Landau level having definite angular momentum

are

$$\varphi_m = \frac{1}{\sqrt{2\pi\ell^2 2^m m!}} z^m e^{-\frac{1}{4}|z|^2} \tag{2.41}$$

where $z = \zeta/\ell$ is a dimensionless complex number representing the position vector $\mathbf{r} \equiv (x, y)$ and $m \geq 0$ is an integer. (Note that $\bar{z}$, the complex conjugate to z, does not appear in the preexponential factor.)

As we anticipated, these wavefunctions are also eigenfunctions of the operator Λ_z and their angular momentum eigenvalue is $\hbar m$. If we restrict our attention to the lowest Landau level, then there exists only one state with any given angular momentum and only non-negative values of m are allowed. This 'handedness' is a result of the chirality built into the problem by the magnetic field.

It seems rather peculiar that in the Landau gauge we had a continuous one-dimensional family of basis states for this two-dimensional problem. Now we find that in a different gauge, we have a discrete one dimensional label for the basis states. Nevertheless, we still end up with the correct density of states per unit area as the peak value of $|\varphi_m|^2$ occurs at a radius of $R_{\text{peak}} = \sqrt{2m\ell^2}$. The area $2\pi\ell^2 m$ of a circle of this radius contains m flux quanta. Hence we obtain the standard result of one state per Landau level per quantum of flux penetrating the sample.

2.2 What Happens to Landau Levels in a Unidirectional Periodic Potential.

The effect of a periodic potential on the behavior of electrons confined to a plane and split into highly degenerate Landau levels by a uniform magnetic field has been studied on many occasions [2, 3, 4]. In the Landau gauge (2.28) an electron in a periodic potential is described by:

$$H = \frac{1}{2m}\left(p_x^2 + (p_y + \frac{e}{c}Bx)^2\right) + V_0 \cos Qx \tag{2.42}$$

The eigenfuctions of this Hamiltonian are of the form:

$$\psi_k(x, y) = e^{iky} f_k(x). \tag{2.43}$$

Since the problem is still translationally invariant in the $\hat{y}$ direction, the guiding center coordinate remains a good quantum number just as in unmodulated case. f_k's are eigenfunctions of the one-dimensional Hamiltonian:

$$H_k = \frac{1}{2m}p_x^2 + \frac{1}{2}m\omega_c^2\left(x + k\ell^2\right)^2 + V_0 \cos Qx \tag{2.44}$$

Using the wavefunctions of the N^th Landau level of the unmodulated system (as in 2.35) as a basis set, the calculation of the matrix elements of the modulating potential

gives:

$$V_{N'N}(X) = V_0 \left(\frac{N'!}{N!}\right)^{\frac{1}{2}} e^{-\frac{Q^2\ell^2}{4}} \left(\frac{Q^2\ell^2}{2}\right)^{(N-N')/2} L_{N'}^{N-N'}\left(\frac{Q^2\ell^2}{2}\right) Re(e^{iQX}\, i^{N-N'}). \tag{2.45}$$

where $L_{N'}^{N-N'}(x)$ is a Laguerre polynomial [74].

The resulting energy spectrum has been numerically calculated in [4]. They found that for realistic values of the Fermi energy ($\approx$ 10 meV) and $B > 0.1T$ the first order perturbation theory result, given by the diagonal elements of the hamiltonian:

$$E_N(X) = \hbar\omega_c(N - \frac{1}{2}) + V_0 e^{-\frac{Q^2\ell^2}{4}} L_N\left(\frac{Q^2\ell^2}{2}\right)\cos(QX) \tag{2.46}$$

gives an excellent approximation for large quantum numbers.

The periodic potential lifts the degeneracy of the Landau levels and leads to Landau bands of finite width. The bandwidth ($\approx 2V_0 e^{-\frac{Q^2\ell^2}{4}} L_N(\frac{Q^2\ell^2}{2})$) actually depends on the band index in an oscillatory manner. This is a consequence of the properties of the Laguerre polynomials. Physically it reflects the fact that with increasing N, the spatial extent of the wavefunction increases as $R_c = \sqrt{2N+1}\ell$ as in (2.36). In effect, each electron senses the average of the periodic potential over an interval of width $2R_c$.

The change in energy of electrons in a half-filled Landau level with guiding centers stretching from $-X/2$ to $X/2$ due to the modulation potential is given by the average

of the potential over the interval Λ.

$$\Delta E_{\Lambda} = \frac{V_0 e^{-\frac{Q^2\ell^2}{4}} L_N(\frac{Q^2\ell^2}{2})}{Q\Lambda} \sin\left(\frac{Q\Lambda}{2}\right) \tag{2.47}$$

If the same number of electrons are allowed to occupy a narrower region in the real space (raising the local filling factor to one), for instance, from $-\Lambda/4$ to $\Lambda/4$ the associated energy cost comes to

$$\Delta E_{\Lambda/2} = \frac{2V_0 e^{-\frac{Q^2\ell^2}{4}} L_N(Q^2\ell^2/2)}{Q\Lambda} \sin\left(\frac{Q\Lambda}{4}\right) \tag{2.48}$$

The former state is uniform, while the latter can be thought of as a stripe. Therefore, for noninteracting electrons the energy difference between the ordered stripe and the uniform state, i.e. the cohesive energy of the noninteracting stripe is:

$$\Delta E_{\Lambda/2} - \Delta E_{\Lambda} = \frac{V_0 e^{-\frac{Q^2\ell^2}{4}} L_N(\frac{Q^2\ell^2}{2})}{Q\Lambda} \left(2\sin\left(\frac{Q\Lambda}{4}\right) - \sin\left(\frac{Q\Lambda}{2}\right)\right) \tag{2.49}$$

Chapter 3

The Ground State of Interacting Electrons in Moderate Magnetic Fields.

A zebra is a light-colored animal with dark stripes:

not a dark one with light stripes.[1]

[1] American Museum of Natural History [65]. After discovery in South Africa that dark parts of zebras fade while light parts remain unchanged.

Overview.

This chapter is devoted to the exposition of experimental and theoretical results that lead to current understanding that two-dimensional electrons in a weak magnetic field at half filling in an upper Landau level organize themselves into a stripe state. In section (Sec. 3.1) I discuss one of the experiments performed by J. Eisenstein's group that clearly demonstrated the novel physics of the system.

In Sec. 3.2 I summarize the foundation of basic assumptions that allow one to proceed with the derivation of the stripe ground state in Sec. 3.6.1.

In the latter section I show how the screened interaction combined with the structure of one-particle states in higher Landau levels leads to the formation of the guiding center charge density wave. The Hartree-Fock interaction turns out to be short-ranged and, moreover, at certain wavevectors, the exchange part becomes greater than the direct one making the formation of the charge density wave energetically favorable. The logic of the calculations in this section differs from the one originally presented in [11] and is more suitable for the consideration of the system in an additional periodic potential to be considered in Sec. 4.2.

3.1 Experiments: Bumps and Wiggles in the Magnetic Field Dependence of the Resistivity.

New collective phenomena in two-dimensional electron systems have largely been discovered by examining the behavior of the magnetic field dependence of the transport coefficients ρ_{xx} and ρ_{yy}. For instance, the famous $\nu = 1/3$ Fractional Quantum Hall Effect was discovered in [5] by noting the unexpected deep minimum in ρ_{xx} and a plateau in ρ_{yy} at that $\nu = 1/3$.

The same trend has continued and applies to the situation of interest here: anomalies in the resistivity on high Landau levels were noticed as far back as in 1988 [6], [7].

3.1.1 Creating Two Dimensional Electrons: Inversion Layers.

Experimentally two dimensional electrons are realized in *inversion layers*. Inversion layers are formed on the interface between two semiconductors (or a semiconductor and an insulator). GaAs/AlGaAs systems are currently experimenter's combination of choice as it allows the manufacture of two dimensional electron gases where the effect of impurities can be made very small. The basic idea of the inversion layer

is to arrange that an electric field perpendicular to the interface attracts electrons from the semiconductor to it. These electrons sit in a quantum well created by this field and the interface. The motion perpendicular to the interface is quantized and therefore under appropriate conditions only the lowest energy level is occupied. The result is a two-dimensional system of electrons.

In the GaAs/AlGaAs system AlGaAs has a wider band gap and plays a role of the insulator. It is deliberately doped n-type, putting mobile electrons into its conduction band. These electrons will migrate to the bottom of the GaAs conduction band. The positive charge left on the donor impurities will attract these electrons to the interface and bend the bands in the process. This is the source of the electric field in the system. The conduction band bends below the Fermi surface near the insulator-semiconductor interface. This is the *inversion layer*, with the bottom of the of the conduction band below the top of the valence band, inverting the normal order.

One of the major advantages of the GaAs/AlGaAs system from the experimentalist's point of view (see, for instance, M. Cage in [70]) is that it lends itself very well to the molecular beam epitaxy techniques, allowing growth of atomically sharp interfaces called *heterojunctions*. This results in the lowest impurity density, and the lowest density of interface defects available. Another important technique is to implant necessary donors physically away from the interface of the AlGaAs. This is

known as *modulation doping*, and results in almost all of the impurity dopant atoms residing several hundred Angstrom away from the inversion layer. The quality of the samples is conventionally characterized by the electron *mobility* in zero magnetic field. Better samples have higher mobility.

3.1.2 Experimental Evidence of Resistivity Anisotropy.

Figure 3.1.2 from Ref.[9] illustrates the anisotropy of the longitudinal resistance seen in high Landau levels at $T = 50$mK. The sample Lilly *et. al.* used in their experiments is a modulation-doped GaAs/AlGaAs heterojunction containing a two-dimensional electron gas with sheet density of $n = 2.7 \times 10^{11}\text{cm}^{-2}$ and a mobility of 11×10^6 cm^2/Vs. This structure was grown by molecular beam epitaxy on a $\langle 001 \rangle$ GaAs substrate.As the insets suggest, the sample geometry consists of a square mesa, 2.5 mm on a side, etched onto a larger square chip. For the data in Fig. 3.1.2, the solid curve corresponds to current flowing between corner contacts along the diagonal of the square which is parallel to the $\langle 110 \rangle$ crystallographic direction while for the dotted curve the current flow is between corner contacts along the diagonal parallel to $\langle 1\bar{1}0 \rangle$. The inset to the figures identifies these diagonals. For each trace, the measured voltage is that between the two midpoint contacts on one side of the current flow axis. These two orthogonal resistance measurements yield vastly different results when the

two dimensional electron system Fermi level is near half filling of several spin resolved Landau levels. The largest anisotropy Lilly *et. al* observed is in the $N = 2$ LL near $\nu = 9/2$. At this filling a deep minimum was seen when the current is driven along $\langle 110 \rangle$, while a tall peak is found with the current along $\langle 1\bar{1}0 \rangle$. For the data shown, the ratio of these resistances is about 60; in some samples the ratios as high as 3500 have been found. Substantial anisotropies have also been seen at $\nu = 11/2, 13/2$ and several higher half-odd integers. These very large resistivity anisotropies (factor of ~ 7 for the $\nu = 9/2$ data in Fig. 3.1.2) characterize transport in half-filled high ($N \geq 2$) Landau levels. This contrasts sharply with the essentially isotropic transport observed at $\nu = 7/2$ and $5/2$ in the $N = 1$ Landau level (shown in Fig. 3.1.2) and at $\nu = 3/2$ in the $N = 0$ lowest Landau level. Fig. 3.1.2b demonstrates that for currents applied between opposing midpoints of the square, i.e. along the $\langle 100 \rangle$ and $\langle 010 \rangle$ directions, little anisotropy is seen at any filling factor. Collectively, these results show that the principal axes of the transport anisotropy are roughly aligned along the $\langle 110 \rangle$ and $\langle 1\bar{1}0 \rangle$ directions. The origin of this anisotropy is still unknown, but recent experiments [26] estimate the anisotropy energy to be ≈ 1 mK per electron.

Figure 3.1: Transport anisotropy in high Landau levels. a) current flow along $\langle 1\bar{1}0 \rangle$ (dotted) and $\langle 110 \rangle$ (solid). b) current flow along $\langle 010 \rangle$ (dotted) and $\langle 100 \rangle$ (solid). Adapted from Ref. [9].

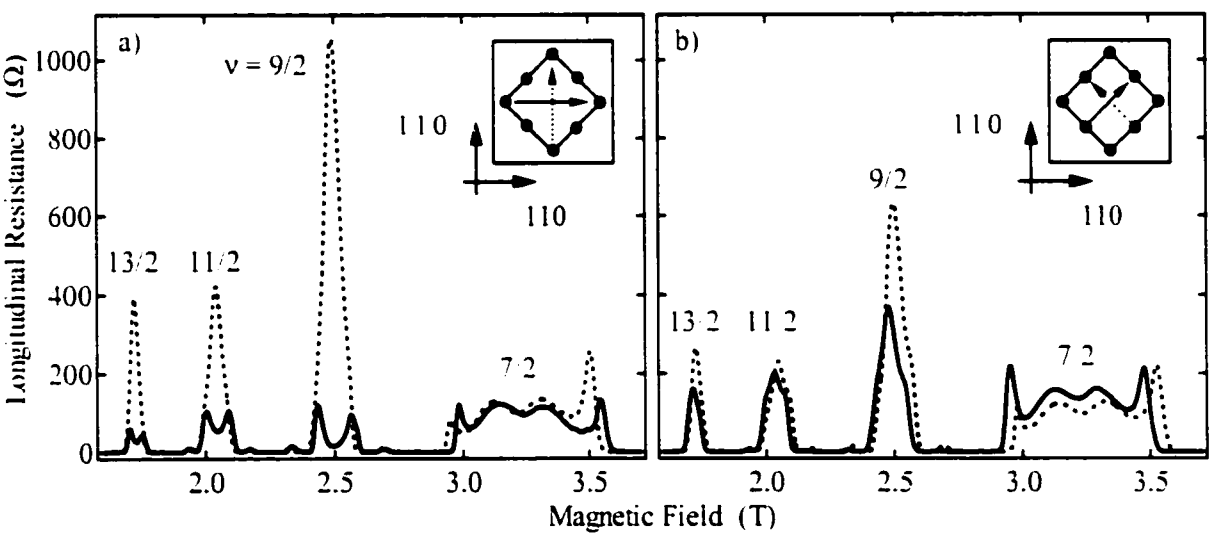

3.2 Why Should One Think about Polarized Electrons Restricted to a Single Landau Level Even in Weak Magnetic Fields?

The main argument regarding the ground state of the system in Sec. 3.6.1 below depends on consideration of spinless electrons restricted to a given Landau level in a clean system. In other words, we will assume that even in weak magnetic fields, where the cyclotron gap $\hbar\omega_c$ is small, the electron-electron interactions do not destroy the Landau quantization and that there is no impurity potential present. Therefore the first order of business is to present the arguments for validity of these assumptions. This is what we will do in sequence. First, we will show that due to screening one can neglect the Landau level mixing. After that we discuss spin excitations. We will argue that energy scale of spin excitations is significantly higher than that of charge excitations. Lastly, we will discuss the role of impurities.

3.2.1 What the Screening Can Do.

The theory of the stripe state strongly relies on the existence of individual Landau levels. This is far from being evident, but has been demonstrated to be true by Aleiner and Glazman [14]. To see that the Landau level mixing is small, one has to

estimate the interaction energy per particle at the upper Landau level and verify that its absolute value is much smaller than $\hbar\omega_c$.

Let us first consider an incompressible electron liquid with an integer filling factor $\nu = 2N$. Because of the gap $\hbar\omega_c$ in the spectrum, an external in-plane electric field $\mathcal{E}$ can not be screened by the 2D electron system. Instead, it causes only a finite polarization per unit area, $\mathcal{P} = \chi\mathcal{E}$. The polarizability of the incompressible 2D electron liquid reduces the interaction $U(r)$ between two point charges embedded into it.

$$U(r) = \int \frac{d^2q}{(2\pi)^2} \frac{2\pi e^2}{\kappa q} \frac{1}{\varepsilon(q)} e^{iqr}. \tag{3.1}$$

where the two-dimensional dielectric function $\varepsilon(q)$ is related to the polarizability χ by [30]

$$\varepsilon(q) = 1 + \frac{2\pi q}{\kappa}\chi(q). \tag{3.2}$$

where κ is the background dielectric constant.

At small wave vectors, the matrix elements of the dipolar moment between electrons in adjacent Landau levels, $d_{N,N-1}$, give the main contribution to the polarizability, $\chi \sim n_L|d_{N,N-1}|^2/\hbar\omega_c$; here

$$n_L = \frac{1}{2\pi l^2} \tag{3.3}$$

is the electron density of a full Landau level (it is just the inverse of the number of

states N_Φ calculated in Eq. (2.37). The characteristic spread of the electron wave function on a high Landau level is equal to the cyclotron radius R_c, and the estimate of the dipolar moment is $d_{N,N-1} \sim eR_c$. Substituting ν into Eq. (3.2), we find:

$$\varepsilon(q) = 1 + \frac{R_c^2}{a_B} q, \tag{3.4}$$

where

$$a_B = \hbar^2 \kappa / me^2 \tag{3.5}$$

is the Bohr radius. Eq. (3.4) is valid only at small wave vectors, $qR_c \ll 1$. In the opposite limit, $qR_c \gg 1$, a large number of Landau levels participate in polarization of the two-dimensional electron liquid. Therefore, the standard Thomas-Fermi screening holds:

$$\varepsilon(q) = 1 + \frac{2}{qa_B}. \tag{3.6}$$

Formulas (3.4) and (3.6) match at $qR_c \sim 1$; the corresponding value of the dielectric constant, $\varepsilon(q \sim 1/R_c) \sim R_c/a_B$, is large ($\sim 10$) in the weak magnetic field limit, where $R_c \gg a_B$. The dielectric function for arbitrary q has been calculated in [14] and is given by Eq. (3.10) below.

As follows from Eq. (3.4), polarization is irrelevant only for interactions on a very large length scale, $r \gg R_c^2/a_B$, where $U(r)$ is given by the unscreened Coulomb interaction. At a smaller scale, $R_c \ll r \ll R_c^2/a_B$, polarization is important.

The renormalized potential is significantly smaller than $\hbar\omega_c$. Therefore, unlike the bare Coulomb potential, the renormalized interaction does not mix Landau levels. Similar to the strong magnetic field case, $\nu < 1$, the corresponding Hamiltonian is just the energy of interaction between the electrons restricted to a single, partially filled Landau level. The main difference is that in the present case the interaction potential (3.1) is much smaller than the bare Coulomb potential, and the electrons are restricted to the partially filled Landau level with a high Landau level index $N \gg 1$ (in practice, we will consider $N \geq 2$).

Because of the strong repulsion between electrons at short distances, one might expect that the interaction of overlapping wavefunctions at these distances gives the main contribution to the energy of the many-electron state. However, for the fully spin polarized electron system of the partially filled Landau level, the orbital part of the many-electron wave function is antisymmetric, and vanishes whenever two electrons have the same coordinates. This suppression of the wave function amplitude compensates the large value of the interaction potential at $r \lesssim a_B$.

3.2.2 What About Spin Excitations?

Let us now turn to the discussion of the spin-flip excitations. The orbital part of the many-electron wave function of such an excited state with one spin flipped is no longer

antisymmetric. Therefore, the energy of such an excitation, is determined not only by the bare Zeeman energy but also by the extra interaction energy associated with the change in the structure of the orbital wave function. Because the orbital part of the wave function is not antisymmetric, the interaction on a short range ($r \lesssim a_B$) now contributes to the energy of the state. This corresponds to the well known exchange enhancement of the g-factor[15]. (The bare value in GaAs is rather small $g \sim 0.013$.) Flipping the spin of a single electron affects the exchange interaction of this electron with all the other electrons of the same Landau level. All the lower Landau levels carry equal number of electrons of both spin polarizations, and do not contribute to the energy associated with the spin flip. Therefore, only $1/2N$-th fraction of the total electron density participates in the exchange enhancement, and the corresponding contribution to energy of the spin-flip is approximately N times smaller than the exchange energy per electron at zero magnetic field. For a two-dimensional electron gas with Fermi wave vector k_F, the latter energy is of the order $e^2 k_F/\kappa$, and the contribution to the energy of a spin-flip is of the order $e^2 k_F/\kappa N$. We see that in the weak magnetic field, the energy scale of charge excitations $\hbar\omega_c/N$ is significantly smaller than the energy scale for spin excitations $r_s\hbar\omega_c$, where

$$r_s = \frac{\sqrt{2}}{k_F a_B} \tag{3.7}$$

This is qualitatively different from the situation at low filling factor, $\nu \lesssim 1$, where both these excitations are characterized by the same energy scale $e^2/\kappa\ell$.

3.3 Why Should There Be a Charge Density Wave?

Usually the direct electrostatic interaction is repulsive and dominates over a weak attraction due to exchange. In our system the Hartree part of the interaction vanishes at the "magic" wavevector because no charge density is induced at that wavevector. As a result, the exchange part of the interaction dominates over the direct one and gives rise to a range of q's around the magic wavevector where the net effective interaction $\tilde{u}_{\rm HF}(q)$ is attractive, which leads to the instability.

The nodes of $F_X(q)$ responsible for the vanishing of $\rho(q)$ exist for a purely geometric reason that the quasiparticle orbitals are extended objects of a specific ring-like shape. The size of the orbitals is uniquely defined by n and ν. These two properties seem to make the position of the global minimum very insensitive to approximations contained in the Hartree-Fock approach as well as many microscopic details, e.g., the functional form of $\epsilon(q)$, thickness of the two dimensional layer, which affects $\tilde{v}_0(q)$, etc [12].

3.4 Stripes vs. Wigner Crystal and Laughlin States.

The charge density wave state turns out to be the most energetically favorable because it represents the correlations on the largest length scale in the problem, R_c. The correlations on the length scale l, built into the structure of, say, the Wigner crystal, are much less effective.

One of the possible particle distributions is the Wigner crystal, i.e., the state where every other lattice site is occupied by an electron. Fogler *et. al.* [11] have shown that the absolute value of its cohesive energy does not exceed u_0, the maximum value of the two-particle interaction potential. (Cohesive energy of any state is the difference between the energy per particle of a that state and the uniform state.) It will be demonstrated below that at $\bar{\nu} = 1/2$ the arrangement of the particles in a series of equidistant large clusters of width $\sim R_c$ (often referred as *stripes*) allows the system to attain the cohesive energy as small as

$$E^0_{coh} = -(3 - 2\sqrt{2})u_0. \tag{3.8}$$

As mentioned above, the reason that the charge density wave has the lowest cohesive energy is because it incorporates correlations at the largest length scale of the problem, R_c. On the other hand, another class of states that could possibly compete with the stripe state is the Laughlin states. They describe the incompressible ground states

at certain filling factors on the lowest Landau level, are thought to take into account correlations on the length scale $\sim \ell \ll R_c$. Numerical simulation of [11, 22] also indicate that the charge density wave has lower cohesive energy than Laughlin liquid for $N \geq 2$.

3.5 Role of Disorder.

In the present work I consider a clean system, i.e. totally neglect the effects of disorder that is inevitably present in real samples. The role of disorder has been studied in a recent paper by D. N. Sheng *et. al.* [28], where numerical diagonalization at different amplitudes of the disorder potential has been performed. Their simulations show that the presence of a very weak random potential associated with disorder does not modify the striped state. However, there exists a critical disorder strength, $\sim 0.12e^2/\kappa\ell$, which marks a transition/crossover from the anisotropic stripe phase at weak disorder strength to an isotropic fluid phase above the critical value, as has been shown in [28].

3.6 The Effect of Screened Interaction on Electrons in a Half-Filled Higher Landau Level: Formation of Stripes.

In this section I proceed with the Hartree-Fock calculation of the ground state and its energy of electrons in a half-filled higher Landau level. This section consists of three subsections:

- The Hamiltonian of interacting electrons is discussed in 3.6.1.
- The Hartree-Fock interaction is derived in 3.6.2.
- In 3.6.3 I discuss the charge density wave order parameter and calculate the cohesive energy of the stripe state.

3.6.1 Hamiltonian of the Interacting Electrons Projected on a Given Landau Level.

Our objective is to find the ground state of electrons in an arbitrary half-filled higher Landau level. Until Sec. (3.6.3) there is no need to restrict ourselves to a particular filling fraction of the partially occupied Landau level, which we denote $\bar{\nu} = \nu - 2N$.

There are N fully filled Landau levels below, with two spin sublevels on each, that screen Coulomb interactions of the partially filled Landau level as discussed above.

In the Landau gauge $\mathbf{A} = -Bx\hat{y}$ electronic wavefunctions are labelled by the guiding center coordinate X and are given by:

$$\Psi_N(x,y) = \frac{e^{iyX/\ell^2}}{\pi^{1/4}\sqrt{2^N N!\ell L_y}} \exp\left[-\frac{(x-X)^2}{2\ell^2}\right] H_N\left(\frac{x-X}{\ell}\right)$$

as we have seen in Sec. (2.1), Eq. (2.35).

Fogler *et al.* [11] have shown and we will now recall, that due to the screening of the inter-electron interaction by the lower filled Landau level electrons, the ground state in the partially filled Landau level is the CDW and can be described in the Hartree-Fock approximation. The Hamiltonian governing the low-energy physics of the two-dimensional liquid in a weak magnetic field is given by:

$$H^0_{eff} = \frac{1}{2L_x L_y}\sum_{\mathbf{q}} \rho(\mathbf{q})\frac{2\pi e^2}{\varepsilon(q)q}\rho(-\mathbf{q}) \tag{3.9}$$

Here $2\pi e^2/q$ is the two-dimensional Fourier transform of the Coulomb interaction

$$\int d^2\mathbf{r}\frac{e^{-i\mathbf{q}\mathbf{r}}}{r} = 2\pi\int dr J_0(qr) = \frac{2\pi}{q},$$

where, as before, $\varepsilon(q)$ the dielectric coefficient of the system with the background dielectric constant κ [14]:

$$\varepsilon(q) = \kappa\left(1 + \frac{2}{qa_B}\left[1 - J_0^2(qR_c)\right]\right). \tag{3.10}$$

Here $J_0(x)$ is the Bessel function [74]. R_c is the cyclotron radius (2.36). r_s is the conventional interaction strength parameter introduced in (3.7). and a_B is Bohr radius (3.5).

The density operator projected on the upper Landau level $\rho(\mathbf{q})$ has the form (see Appendix A for details):

$$\rho(\mathbf{q}) = \sum_X F(q) e^{-iq_x X} a^\dagger_{X_+} a_{X_-}.$$

where $a^\dagger_X$ (a_X) is the creation (annihilation) operator of the state Ψ_X, (see Eq. (2.35)) and $X_\pm = X \pm q_y \ell^2/2$. $F(q)$ is the form factor of the state Ψ_X:

$$F(q) = \exp\left(-\frac{q^2\ell^2}{4}\right) L_X\left(\frac{q^2\ell^2}{2}\right)$$

$L_X(x)$ is the Laguerre polynomial [74]. It is important that the density operator is modulated by $F(q)$, due to oscillatory nature of electronic wavefunctions on higher Landau levels. The form-factor plays an essential role in reducing the reach of the Coulomb interaction.

3.6.2 Electron-Electron Interaction in the Hartree-Fock Approximation.

One of the important insights of [11] was to consider the average *guiding center* density as the order parameter. This order parameter is introduced below.

The Hartree-Fock decoupling (for details see Appendix B) proceeds with the guiding center order parameter $\tilde{\Delta}(\mathbf{q})$ defined as:

$$\tilde{\Delta}(\mathbf{q}) = \frac{2\pi\ell^2}{L_x L_y} \sum_X e^{-iq_x X} \langle a^\dagger_{X-} a_{X-} \rangle \tag{3.11}$$

It is essential that the form factor has been moved from the expression for the electron density to become part of the effective interaction as will be seen below.

The Hartree-Fock decoupled Hamiltonian (3.9) takes on the form:

$$H^0_{HF} = \frac{n_L}{2} \sum_{\mathbf{q}} \tilde{u}^{eff}_{HF}(q) \Delta(\mathbf{q}) \sum_X e^{-iq_x X} a^\dagger_{X-} a_{X-}. \tag{3.12}$$

where $n_L = \frac{1}{2\pi\ell^2}$ is the electron density of a full Landau level that has been introduced in (3.3). The Hartree-Fock interaction potential is the difference between its direct (Hartree) and exchange (Fock) parts: $\tilde{u}^{eff}_{HF}(q) = \tilde{u}_H(q) - \tilde{u}_F(q)$. The Hartree part of the potential is given by:

$$\tilde{u}_H(q) = \frac{2\pi e^2 F^2(q)}{\varepsilon(q) q}. \tag{3.13}$$

while the Fock potential turns out to be proportional to the Fourier transform of the Hartree potential, (see Appendix B for details):

$$n_L \tilde{u}_F(q) = u_H(q\ell^2) \tag{3.14}$$

the interaction potential, at $r_s \sim 1$, $R_c^{-1} \leq q \ll k_F$ can be approximated by [11]:

$$n_L \tilde{u}^{eff}_{HF}(q_x, q_y) \approx \frac{\hbar\omega_c}{\pi^2} \frac{\sin(2R_c\sqrt{q_x^2 - q_y^2})}{2R_c\sqrt{q_x^2 - q_y^2}}. \tag{3.15}$$

The main tool employed in this work to discriminate between competing ground states will the value of these states' cohesive energy.

By *cohesive energy* we understand the difference between the energy per particle of a candidate state and the uniform state. The value of cohesive energy is obtained by dividing the expectation value of the corresponding Hamiltonian by the number of particles in the Landau level, $\bar{\nu} n_L L_x L_y$ and subtracting the energy per particle in the uniform state.

The ground state is determined by the CDW parameter $\Delta(q_x, q_y)$ that minimizes the cohesive energy:

$$E^0_{coh} = \frac{n_L}{2\bar{\nu}} \sum_{\mathbf{q}\neq 0} \tilde{u}^{eff}_{HF}(q_x, q_y) |\Delta(\mathbf{q})|^2 \tag{3.16}$$

$\bar{\nu}$ is the average filling factor equal to $\frac{1}{2}$ for half filled Landau levels considered here. $\mathbf{q} = 0$ term is the energy per particle in the uniform state and therefore has been subtracted.

3.6.3 Formation of Stripes.

Fogler *et. al.* [11] proposed that the ground state of the Hamiltonian (3.9) with the potential (3.15) at the filling factor $\bar{\nu} = 1/2$ should be a charge density wave with occupied states whose guiding center coordinates fall within certain range and the rest empty. This is often referred to as a *stripe* state.

In other words, the stripe state ansatz is the statement that

$$\langle a_X^\dagger a_X \rangle = \delta(q_y) \text{ for } (n - 1/4)\Lambda < X < (n + 1/4)\Lambda.$$

where Λ is the period of the presumed charge density wave (we will assume that $M = \frac{L_x}{\Lambda}$ is the total number of the stripes) and n is an integer labelling the stripe. This implies the following expression for the order parameter (3.11):

$$\tilde{\Delta}_0(q_x, q_y) = \frac{2\pi\ell^2}{L_x L_y} \sum_X e^{-iq_x X} \langle a_{X-}^\dagger a_{X-} \rangle = \frac{2\pi\ell^2}{L_x L_y} \sum_n \int_{(n-1/4)\Lambda}^{(n+1/4)\Lambda} \frac{L_y}{2\pi\ell^2} dX e^{-iq_x X} \delta(q_y) =$$

$$= \frac{M}{L_x} \int_{-\Lambda/4}^{\Lambda/4} dX e^{-iq_x X} \delta(q_y) = \frac{2}{\Lambda q_x} \sin\left(\frac{\Lambda q_x}{4}\right) \delta(q_y). \tag{3.17}$$

where q_x is an integer multiple of $\frac{2\pi}{\Lambda}$. Here and below we denote the order parameter with the symbol Δ and its Fourier transform in q-space with $\tilde{\Delta}$. (Tilde will carry a meaning of the Fourier transform for other functions as well.) Switching to the real space, we obtain the following expression for the cohesive energy:

$$E_{coh}^0 = \frac{n_L L_x L_y}{2\bar{\nu}} \int dx dy \int dx' dy' u_{HF}^{eff}(x - x') \Delta_0(x') \left(\Delta_0(x) - \frac{\bar{\nu}}{L_x L_y} \right). \tag{3.18}$$

where the order parameter is the Fourier transform of $\tilde{\Delta}_0(q_x, q_y)$ above:

$$\Delta_0(x) = \frac{\Theta(\Lambda/4 - |x|)}{L_x L_y}. \tag{3.19}$$

That is, $\Delta_0(x) = 1/L_x L_y$ for $-\Lambda/4 \leq x \leq \Lambda/4$ with the period Λ and zero elsewhere. The Fourier transform is performed by changing the order of integration as shown

below:

$$\int_0^{\frac{L_x}{\ell^2}} \frac{dq_x}{2\pi} \frac{e^{iq_x(\Lambda/4+x)} - e^{-iq_x(\Lambda/4-x)}}{iq_x} =$$

$$= \frac{1}{2\pi} \int_0^{\frac{L_x}{\ell^2}} dq_x \left(\int_{-x}^{\Lambda/4} d\eta e^{iq_x(\eta+x)} + \int_{x}^{\Lambda/4} d\eta' e^{-iq_x(\eta'-x)} \right)$$

$$= \int_{-x}^{\Lambda/4} d\eta \delta(\eta + x) + \int_{x}^{\Lambda/4} d\eta' \delta(\eta' - x) = \int_{-\Lambda/4}^{\Lambda/4} d\eta \delta(\eta - x) = \Theta(\Lambda/4 - |x|)$$

The stripes can be pictured as shown on the Figure 3.2. Since the order parameter is y independent, reflecting the uniformity of the stripes in the y direction, one obtains the Hartree-Fock interaction (3.15) in real space in the form:

$$n_L u_{HF}^{eff}(x) = \frac{\hbar\omega_c}{2\pi^2 R_c} \Theta(2R_c - |x|) \equiv u_0 \Theta(2R_c - |x|). \tag{3.20}$$

where we have introduced

$$u_0 = \hbar\omega_c / 2\pi^2 R_c \tag{3.21}$$

Notice that the strength of the interaction potential has the dimensionality of energy over length. (To obtain the total energy I will be integrating twice over distance and this will restore the usual units.) In the expression for the Hartree-Fock potential we have omitted the contact part of the potential that is unimportant for our discussion.

Calculation of the cohesive energy is now a simple matter.

$$E_{coh}^0 = \frac{1}{2\bar{\nu}} \sum_{n,n'} \int_0^{L_x} \frac{dx}{L_x} \int_0^{L_x} dx' u_0 \Theta(2R_c - |x - x'|) \Theta(\Lambda/4 - |x' - n'\Lambda|) \times$$

$$\left(\Theta(\Lambda/4 - |x + n\Lambda|) - \frac{1}{2} \right)$$

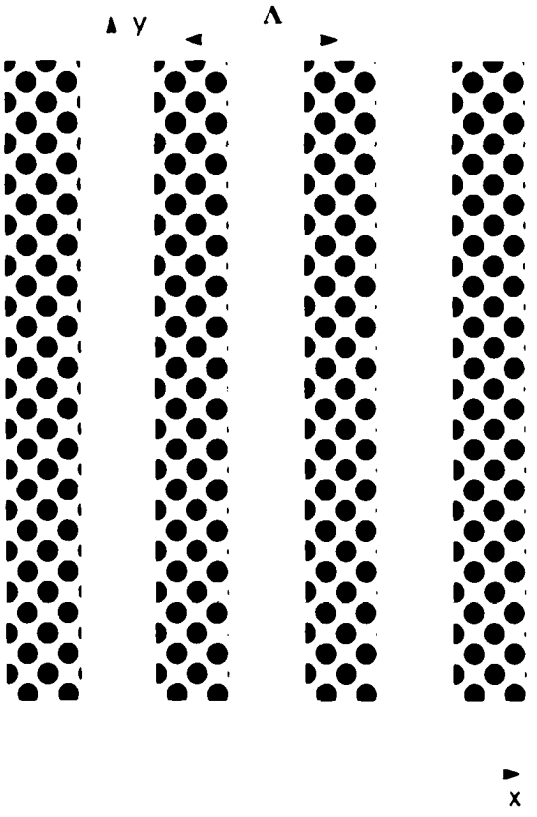

Figure 3.2: Geometry of unperturbed stripes: the stripes are uniform in the $\hat{y}$ direction and periodic with the period Λ in the $\hat{x}$ direction.

Due to the symmetry of the integral, it breaks up into M (the number of stripes) integrals. Therefore the cohesive energy can be rewritten as

$$E^0_{coh} = \frac{1}{2\bar{\nu}} \int \frac{dx}{\Lambda} \int dx' u_0 \Theta(2R_c - |x - x'|) \Theta(\Lambda/4 - |x'|) \left(\Theta(\Lambda/4 - |x|) - \frac{1}{2} \right) \quad (3.22)$$

We will use the fact that the cohesive energy has the form of this type of average again in Sec. 4.2.1.

The integral involved here is a particular case ($f \equiv 1$) of the integral considered in the Appendix C. Using this expression one obtains for the cohesive energy

$$E^0_{coh} = u_0 \frac{\Lambda^2/2 - 3\Lambda R_c + 4R_c^2}{\Lambda} \tag{3.23}$$

Recall, that our objective is to minimize this expression for the cohesive energy. One can proceed either by considering the cohesive energy to be a function of the period of the stripes, finding Λ such that $\partial E^0_{coh}(\Lambda)/\partial\Lambda = 0$, and then calculating $E^0_{coh}(\Lambda)$ at this value of the period. This is how the results described below were originally obtained in [11]. However, I shall take a slightly different approach as it is the way the more general problem will be approached in Sec. 4.2.

Introducing the further notation,

$$\epsilon_0 = E^0_{coh}/u_0 \tag{3.24}$$

we consider the expression above as a quadratic equation for $\Lambda(\epsilon_0)$

$$\frac{\Lambda^2}{2} - (3R_c - \epsilon_0)\Lambda + 4R_c^2 = 0$$

with the solutions:

$$\Lambda = 3R_c \pm \sqrt{\epsilon_0^2 - 6\epsilon_0 R_c - R_c^2}$$

The minimal value of the cohesive energy is obtained by observing that the existence of real and positive period of the stripes requires that

$$\epsilon_0^2 + 6\epsilon_0 R_c - R_c^2 \geq 0. \tag{3.25}$$

Only the positive root of this equation satisfies these conditions. Therefore, as quoted above in Eq. (3.8):

$$\epsilon_0 = -(3 - 2\sqrt{2})R_c \text{ and} \tag{3.26}$$

$$\Lambda = 2\sqrt{2}R_c \tag{3.27}$$

In this section I have reviewed the results of the article [11] that demonstrate that the ground state of electrons in higher Landau levels is a guiding center charge density wave with the period $\Lambda \equiv 2\sqrt{2}R_c$. The ground state energy of this state is lower than the energy of the uniform state by the amount $\epsilon_0 \equiv (-3 + 2\sqrt{2})R_c$.

To recapitulate, starting with the order parameter, Eq. (3.17) or (3.19), we have found the cohesive energy of the half-filled Landau level in such a state as a function of the width of a stripe. The self-consistency condition on the existence of a stripe expressed by the Eq. (3.25) led us to the minimal value of the cohesive energy quoted above.

Chapter 4

Higher Landau Level Stripes in a Periodic Potential.

But still. my homeward way has proved too long.

While we were wasting time there. old Poseidon.

it almost seems. stretched and extended space.

Joseph Brodsky

Odysseus to Telemachus

4.1 Experiment: Resistivity in Short-Period Unidirectional Lateral Superlattices.

An interplay between artificial periodicity of a lateral superlattice introduced into two-dimensional electron gas and the cyclotron radius of electrons is known to give rise to magnetoresistance oscillations, known as Weiss oscillations [24]. Weiss oscillations are observed at magnetic fields B of the order $\sim 0.5T$ when the cyclotron diameter is of the order of several hundred nanometers. At these fields the Landau quantization does not play an important role.

To pursue the interplay between the artificial periodicity and the electron dynamics in the quantum Hall regime A. Endo *et. al.* [23] have created superlattices with the period $a = 92$ nm and investigated its influence on the magnetoresistance near $\nu = 9/2$ filling fraction. In the experiment, GaAs/AlGaAs two dimensional electron gas with the mobility $\mu = 7.6 \times 10^5 cm^2/(Vs)$ at 4.2 K and electron density $n = 2.1 \times 10^{11} cm^{-2}$ is fabricated into Hall bars. (Notice that the mobility in these samples is over an order of magnitude lower that in the experiments discussed in Sec. 3.1.) These bars were further prepared into lateral superlattices with two different direction of grating with respect to the direction of current. The perpendicular lateral superlattices have a grating with the direction of modulation along the current, see

insert on Fig. 4.1. And parallel superlattices, where the direction of modulation is perpendicular to the current, see insert on Fig. 4.2. In both cases the current axis is along ⟨110⟩ direction. The authors estimate that the amplitude of the modulation is $V_0 = 0.015$ meV, or 0.2 % of the Fermi energy.

Fig. 4.1(a) shows the magnetoresistance traces of the perpendicular superlattice around $\nu = 9/2$ taken at four different temperatures, from $\sim$ 20 mK to 350 mK. The magnetic field for the exact $\nu = 9/2$ filling is 1.93 ± 0.03 T. The figure shows shallow and wide minimum with shoulders on both sides, marked by vertical dotted lines. The peaks become broader with increasing temperature. The less evident peak on the side of the lower field becomes more pronounced in the field derivative traces shown on Fig. 4.1(b).

Magnetoresistance traces for the parallel superlattice are shown on Fig. 4.2. A small peak at $\sim$ 1.97 T corresponds to the minimum for the perpendicular superlattice.

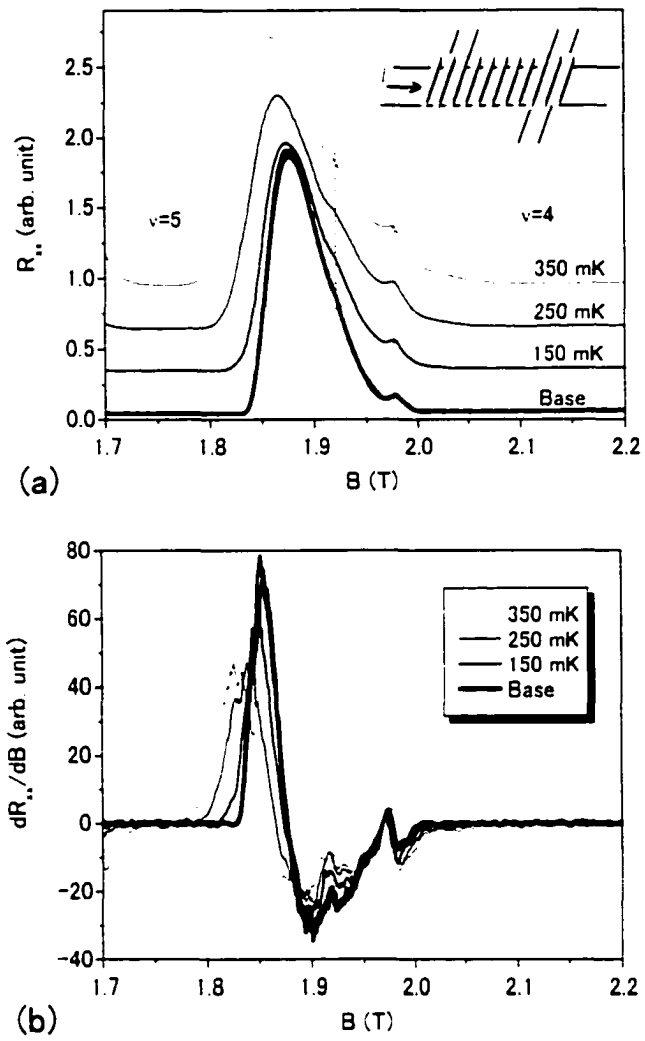

Figure 4.1: (a) Magnetoresistance traces around $\nu = 9/2$ of the perpendicular lateral superlattice (a = 92 nm) at four different (bath) temperatures (I = 100 nA). Traces for higher temperatures are vertically shifted (0.3 units each) for clarity. Vertical dotted lines mark the positions of peaks (or shoulders) which flank both ends of a shallow and broad dent. (b) Derivative of traces in (a). Adapted from Ref. [23].

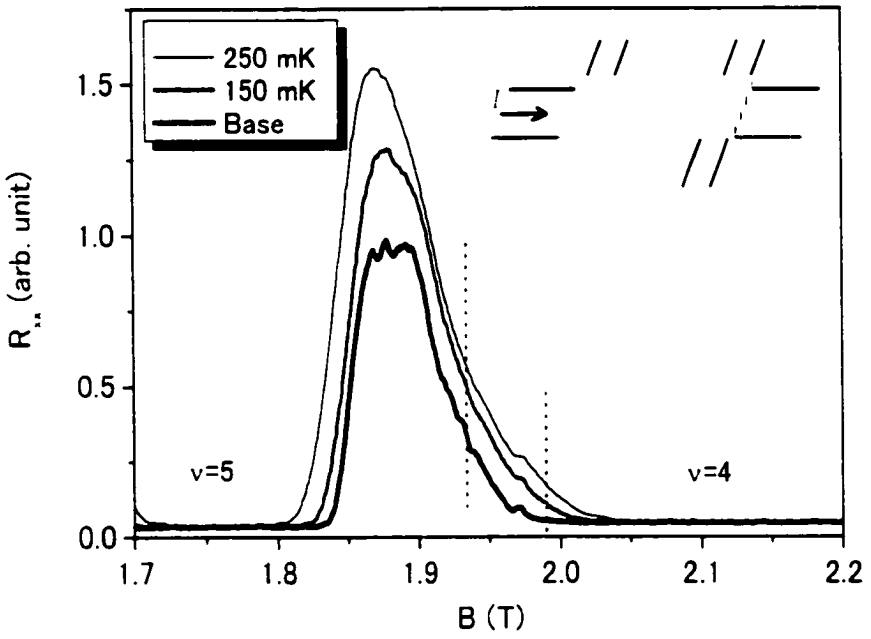

Figure 4.2: Magnetoresistance traces around $\nu = 9/2$ of the parallel lateral superlattice (a = 92 nm) at three different (bath) temperatures (I = 100 nA). Vertical dotted lines indicate the positions of flanking peaks in the perpendicular lateral superlattice, multiplied by a factor 1.007 to correct for slight difference in the electron densities. Adapted from Ref. [23].

Overview.

We turn our attention to the following question: "How do the stripes adjust to the external periodic potential?" We also discuss the influence of the external periodic potential on the transport properties of the modulated stripes. This chapter is the locus of main results presented in this work.

With the external potential present we need to find a modified order parameter that would minimize the cohesive energy including the external potential.

I will start, in Sec. 4.2, with the potential applied perpendicular to the stripes. In this case each stripe can expand or shrink as well as move as a whole with respect to their unperturbed positions to take advantage of the external potential. Therefore we allow for arbitrary changes in widths and positions of the stripes and minimize the cohesive energy with respect to these changes. In Sec. 4.2.1 I find the cohesive energy with the modified order parameter that reflects the influence of the external periodic potential. The consistency of the solution determines the minimal value of the cohesive energy. In the following section, Sec. 4.2.2 I examine the value of the cohesive energy in the limit when the external potential has a very long wavelength. I also find the value of the period of the external potential that gives maximal energy gain for the perpendicular alignment.

Then, in Sec. 4.3, I will consider the potential applied along the stripes. The

periodic potential splits the Landau level into a series of levels corresponding to each reciprocal wavevector. And under these circumstances the stripes can take advantage of the periodic potential by mixing in contributions from these higher energy levels and adjusting their widths.

In Sec. 4.4 I will be able to compare cohesive energies of these two alignments.

In the last section of this chapter, Sec 4.5 I will consider possible experimental signatures of perpendicular alignment.

4.2 Stripes Aligned Perpendicular to the Periodic Modulation.

We continue considering a clean fully spin polarized two-dimensional electron system but now place it in a weak periodic potential. The external potential will be taken to be of the form:

$$V(x) = V_0 \cos(Q_x x).$$

where $2\pi/Q_x$ is the period of the external modulation.

The Hamiltonian that we consider has the form:

$$H_{eff} = \frac{1}{2L_x L_y} \sum_{\mathbf{q}} \rho(\mathbf{q}) \frac{2\pi e^2}{\epsilon(q) q} \rho(-\mathbf{q}) + \sum_{\mathbf{q}} \frac{V_0 F(q)}{2} \rho(\mathbf{q}) \delta(q_x \pm Q_x) \delta(q_y). \qquad (4.1)$$

This is the Hamiltonian of two-dimensional electrons restricted to a partially filled Landau level (3.9) in the external periodic potential.

Our goal, as before, is to minimize the cohesive energy of the interacting stripes in the external potential by allowing stripes to adjust their widths and positions.

The cohesive energy, similarly to (3.16), now takes on the form:

$$E_{coh} = \frac{1}{2\bar{\nu}} \sum_{\mathbf{q}\neq 0} n_L \tilde{u}^{eff}_{HF}(q_x, q_y) |\tilde{\Delta}(\mathbf{q})|^2 + \\ + \frac{V_0 F(q)}{2} \left(\tilde{\Delta}(\mathbf{q}) \exp(-io) + \tilde{\Delta}(-\mathbf{q}) \exp(io) \right) \delta(q_x - Q_x). \qquad (4.2)$$

where we have introduced o, an arbitrary phase of the potential with respect to the origin.

Rewriting (4.2) in real space

$$E_{coh} = \frac{1}{2\bar{\nu}} \int dx \int dx' n_L L_x L_y u^{eff}_{HF}(x - x') [\Delta(x') + \\ + V_0 F(Q_x) \cos(Q_x x + o)] \left(\Delta(x) - \frac{1}{2L_x} \right). \qquad (4.3)$$

we have everything necessary to proceed further.

4.2.1 Cohesive Energy for the Perpendicular Alignment.

We now calculate the cohesive energy of the stripes, but no longer assuming strict periodicity, i.e allowing for arbitrary positions of stripe edges. Once we have the

expression for the cohesive energy, we will, in a similar to the calculations of Sec. 3.6.3 manner, determine the *minimal* value of the cohesive energy from the consistency condition. (The consistency condition for the existence will again be the nonnegativity of a discriminant.)

Let us call the position of the left and right edges of the n^{th} stripe Λ_{2n} and Λ_{2n+1} respectively. This is shown on the figure 4.3. With these notations the calculation of the cohesive energy of the stripe n from (4.3) leads to (see Eq. (3.22) for comparison):

$$E_{coh} = \left[u_0 \left\{ \frac{1}{2}(\Lambda_{2n} - \Lambda_{2n-1})^2 + (\Lambda_{2n+1} - \Lambda_{2n})^2 + \frac{1}{2}(\Lambda_{2n-2} - \Lambda_{2n+1})^2 - \right.\right.$$
$$\left. -2R_c(\Lambda_{2n-2} + \Lambda_{2n} - \Lambda_{2n+1} - \Lambda_{2n-1}) + 4R_c^2 \right\} -$$
$$\left. - \frac{2V_0 F(Q_x)}{Q_x} \sin Q_x \left(\frac{\Lambda_{2n+1} - \Lambda_{2n}}{2} \right) \cos \left(Q_x \frac{\Lambda_{2n+1} + \Lambda_{2n}}{2} + \phi \right) \right] \times$$
$$(\Lambda_{2n-2} + \Lambda_{2n+1} - \Lambda_{2n} - \Lambda_{2n-1})/2]^{-1} - u_0 R_c - \frac{V_0 F(Q_x)}{Q_x \Lambda} \sin Q_x \frac{\Lambda}{2} \qquad (4.4)$$

The last two terms in the this expression represent the energy of the uniform electron gas. To simplify notations we introduce the following variables that will be used throughout:

$$\epsilon = E_{coh}/u_0 \qquad (4.5)$$

for the reduced cohesive energy and

$$v = V_0 F(Q_x)/u_0 \qquad (4.6)$$

for the amplitude of the potential, where u_0 has been introduced in (3.21) Notice

that all variables, including both ϵ and c, now have the dimension of length. We also relabel $\Lambda_s \to \Lambda_s - o/Q_x$. This shift allows us to set o to zero in the following discussion.

In our subsequent analysis we will assume that the ratio of the amplitude of the potential to the strength of the electron-electron interaction is the smallest parameter in the system. We will also consider the potential with the period no less than the stripe period. In our new notations these assumptions take on the form:

$$\frac{c}{\Lambda} \ll Q_x \Lambda \lesssim 1 \tag{4.7}$$

As we have seen, in the absence of the external potential, for $c = 0$, the stripes are equally spaced with $\Lambda_{2n} = (n - 1/4)\Lambda$ and $\Lambda_{2n-1} = (n - \frac{1}{4})\Lambda$. With weak, but nonzero external potential strength, we expect the stripe width and position to change as the stripes adjust to the potential. To take into account both the change in the stripe position and width we introduce the following parameterization (a_{2n}, a_{2n-1}):

$$\Lambda_{2n} = (n - \frac{1}{4})\Lambda + a_{2n} \text{ and } \Lambda_{2n-1} = (n + \frac{1}{4})\Lambda + a_{2n-1} \tag{4.8}$$

This parameterization is illustrated on Fig. 4.3. Our strategy is to look for the solutions of the equation (4.4) for arbitrary values of the cohesive energy ϵ and then find the minimal value of the cohesive energy when solutions of the form (4.8) are possible.

To this end we go to the continuum limit, i.e. promote n to the status of a continuous variable x and introduce $f(x) = a_{2n}$. The position of the left edge of the n^{th} stripe is then $\Lambda_{2n} = (x - \frac{1}{4})\Lambda + f(x)$ and of the right edge $\Lambda_{2n+1} = (x + \frac{1}{4})\Lambda + f(x) + 1/2 f'(x)$. Using (4.8) and rewriting (4.4) as a differential equation for $f(x)$ we get:

$$\frac{1}{2}f'(x)^2 - (\epsilon - \epsilon_0)(f'(x) + \Lambda) + \frac{2v}{Q_x}\sin Q_x\left(\frac{\Lambda + f'(x)}{4}\right)\cos Q_x(\Lambda x + f(x)) - \\ - \frac{v}{Q_x}\sin\frac{Q_x\Lambda}{2}\left(1 + \frac{f'(x)}{\Lambda}\right) = 0.$$

where ϵ_0 was introduced in (3.24).

Moreover, since corrections to the initial stripe positions a_{2n} (and, consequently, $f(x)$) will be seen to be proportional to $\sqrt{v}$, the nonlinear terms can be expanded.

Finally, we obtain the following equation for the shifts of the stripes' edges:

$$\frac{1}{2}f'(x)^2 - \left\{\epsilon - \epsilon_0 - \frac{v}{2}\cos\frac{Q_x\Lambda}{4}\cos Q_x\Lambda x - \frac{2v}{Q_x\Lambda}\sin\frac{Q_x\Lambda}{2}\right\}f'(x) - \\ -(\epsilon - \epsilon_0)\Lambda + \frac{2v}{Q_x}\sin\left(\frac{Q_x\Lambda}{4}\right)\cos Q_x\Lambda x - \frac{v}{Q_x}\sin\frac{Q_x\Lambda}{2} = 0$$

Thus to order v the derivative $f'(x)$ is:

$$f'(x) = \epsilon - \epsilon_0 - \frac{v}{2}\cos\frac{Q_x\Lambda}{4}\cos Q_x\Lambda x - \frac{2v}{Q_x\Lambda}\sin\frac{Q_x\Lambda}{2} \pm \\ \left[\left(\epsilon - \epsilon_0 - \frac{v}{2}\cos\frac{Q_x\Lambda}{4}\cos Q_x\Lambda x + \frac{v}{Q_x\Lambda}\sin\frac{Q_x\Lambda}{2}\right)^2 + \right. \\ \left. + 2(\epsilon - \epsilon_0)\Lambda - \frac{4v}{Q_x}\sin\frac{Q_x\Lambda}{4}\cos Q_x\Lambda x + \frac{2v}{Q_x}\sin\frac{Q_x\Lambda}{2}\right]^{\frac{1}{2}} \qquad (4.9)$$

The condition for the existence of real solutions, namely that the discriminant is nonnegative, determines the minimal value of ϵ when such a solution is allowed (recall our logic that led to Eq. (3.25)). This leads to the following inequality that should hold for any x:

$$(\epsilon - \epsilon_0 + \frac{v}{Q_x.\Lambda} \sin \frac{Q_x.\Lambda}{2})^2 - (\epsilon - \epsilon_0 + \frac{v}{Q_x.\Lambda} \sin \frac{Q_x.\Lambda}{2})(v \cos \frac{Q_x.\Lambda}{4} \cos Q_x.\Lambda x - 2.\Lambda) +$$
$$+ \frac{v^2}{4} \cos^2 \frac{Q_x.\Lambda}{4} \cos^2 Q_x.\Lambda x - \frac{4v}{Q_x} \sin \frac{Q_x.\Lambda}{4} \cos Q_x.\Lambda x \geq 0 \qquad (4.10)$$

Rewrite that as:

$$\Phi(\eta) = (\epsilon - \epsilon_0 + \frac{v}{Q_x.\Lambda} \sin \frac{Q_x.\Lambda}{2})^2 - (\epsilon - \epsilon_0 - \frac{v}{Q_x.\Lambda} \sin \frac{Q_x.\Lambda}{2})(v \cos \frac{Q_x.\Lambda}{4} \eta - 2.\Lambda) +$$
$$+ \frac{v^2}{4} \cos^2 \frac{Q_x.\Lambda}{4} \eta^2 - \frac{4v}{Q_x} \sin \frac{Q_x.\Lambda}{4} \eta \geq 0, \text{ where } \eta \in [-1, 1] \qquad (4.11)$$

with $\eta = \cos Q_x.\Lambda x$. Therefore we have the following set of conditions for $\Phi(1)$, $\Phi(-1)$, and $\Phi(\eta_{min})$ with

$$-1 \leq \eta_{min} = \frac{(\epsilon - \epsilon_0 + \frac{v}{Q_x.\Lambda} \sin \frac{Q_x.\Lambda}{2}) - \frac{4}{Q_x} \tan \frac{Q_x.\Lambda}{4}}{\frac{v}{2} \cos \frac{Q_x.\Lambda}{4}} \leq 1$$

should be nonnegative:

$$\Phi(1) = (\epsilon - \epsilon_0 + \frac{v}{Q_x.\Lambda} \sin \frac{Q_x.\Lambda}{2})^2 - (\epsilon - \epsilon_0 + \frac{v}{Q_x.\Lambda} \sin \frac{Q_x.\Lambda}{2})(v \cos \frac{Q_x.\Lambda}{4} - 2.\Lambda)$$
$$+ \frac{v^2}{4} \cos^2 \frac{Q_x.\Lambda}{4} - \frac{4v}{Q_x} \sin \frac{Q_x.\Lambda}{4} \geq 0. \qquad (4.12)$$
$$\Phi(-1) = (\epsilon - \epsilon_0 + \frac{v}{Q_x.\Lambda} \sin \frac{Q_x.\Lambda}{2})^2 + (\epsilon - \epsilon_0 + \frac{v}{Q_x.\Lambda} \sin \frac{Q_x.\Lambda}{2})(v \cos \frac{Q_x.\Lambda}{4} + 2.\Lambda)$$

$$+\frac{v^2}{4}\cos^2\frac{Q_x.\Lambda}{4}+\frac{4v}{Q_x}\sin\frac{Q_x.\Lambda}{4}\geq 0.\ \text{and} \tag{4.13}$$

$$\Phi(\eta_{min})=(\epsilon-\epsilon_0+\frac{v}{Q_x.\Lambda}\sin\frac{Q_x.\Lambda}{2})\left(2.\Lambda-\frac{8}{Q_x}\tan\frac{Q_x.\Lambda}{4}\right)$$

$$-\left(\frac{4}{Q_x}\tan\frac{Q_x.\Lambda}{4}\right)^2\geq 0 \tag{4.14}$$

The first of the these conditions (4.12) imposes the following restrictions on ϵ:

$$2(\epsilon-\epsilon_0+\frac{v}{Q_x.\Lambda}\sin\frac{Q_x.\Lambda}{2})\geq \varepsilon_1\equiv v\cos\frac{Q_x.\Lambda}{4}-2.\Lambda+$$

$$2.\Lambda\left[1-\frac{v}{\Lambda}\left(\cos\frac{Q_x.\Lambda}{4}-\frac{4}{Q_x.\Lambda}\sin\frac{Q_x.\Lambda}{4}\right)\right]^{\frac{1}{2}} \tag{4.15}$$

or

$$2(\epsilon-\epsilon_0+\frac{v}{Q_x.\Lambda}\sin\frac{Q_x.\Lambda}{2})\leq \varepsilon_2\equiv v\cos\frac{Q_x.\Lambda}{4}-2.\Lambda-$$

$$2.\Lambda\left[1-\frac{v}{\Lambda}\left(\cos\frac{Q_x.\Lambda}{4}-\frac{4}{Q_x.\Lambda}\sin\frac{Q_x.\Lambda}{4}\right)\right]^{\frac{1}{2}} \tag{4.16}$$

The second one (4.13) requires:

$$2(\epsilon-\epsilon_0+\frac{v}{Q_x.\Lambda}\sin\frac{Q_x.\Lambda}{2})\geq \varepsilon_3\equiv -v\cos\frac{Q_x.\Lambda}{4}-2.\Lambda+$$

$$2.\Lambda\left[1+\frac{v}{\Lambda}\left(\cos\frac{Q_x.\Lambda}{4}-\frac{4}{Q_x.\Lambda}\sin\frac{Q_x.\Lambda}{4}\right)\right]^{\frac{1}{2}} \tag{4.17}$$

or

$$2(\epsilon-\epsilon_0+\frac{v}{Q_x.\Lambda}\sin\frac{Q_x.\Lambda}{2})\leq \varepsilon_4\equiv -v\cos\frac{Q_x.\Lambda}{4}-2.\Lambda-$$

$$2.\Lambda\left[1+\frac{v}{\Lambda}\left(\cos\frac{Q_x.\Lambda}{4}-\frac{4}{Q_x.\Lambda}\sin\frac{Q_x.\Lambda}{4}\right)\right]^{\frac{1}{2}} \tag{4.18}$$

Whereas the last condition (4.14) allows ϵ that satisfy:

$$\epsilon - \epsilon_0 + \frac{v}{Q_x\Lambda}\sin\frac{Q_x\Lambda}{2} \geq \varepsilon_5 \equiv -\frac{\Lambda}{2}\frac{\left(\frac{4}{Q_x\Lambda}\tan\frac{Q_x\Lambda}{4}\right)^2}{\frac{4}{Q_x\Lambda}\tan\frac{Q_x\Lambda}{4}-1} \tag{4.19}$$

If

$$\tan\left(\frac{Q_x\Lambda}{4}\right) < \frac{Q_x\Lambda}{2}$$

or, in other words,

$$\frac{Q_x\Lambda}{4} < \frac{10}{27}\pi,$$

i.e. the period of the external potential is greater than a little over Λ, covering most cases of practical interest

$$\varepsilon_2 < \varepsilon_4 < \varepsilon_5 < \varepsilon_3 < \varepsilon_1$$

Therefore the lowest value of the cohesive energy allowed by these conditions is given by ε_1, as illustrated on Fig. 4.4:

$$\epsilon = \epsilon_0 + \left(\frac{v}{2}\cos\frac{Q_x\Lambda}{4} - \frac{v}{Q_x\Lambda}\sin\frac{Q_x\Lambda}{2}\right) - \Lambda + \Lambda\left[1 - \frac{v}{\Lambda}\left(\cos\frac{Q_x\Lambda}{4} - \frac{4}{Q_x\Lambda}\sin\frac{Q_x\Lambda}{4}\right)\right]^{\frac{1}{2}} \tag{4.20}$$

To the second order in v this value is

$$\epsilon = \epsilon_0 + \frac{v}{Q_x\Lambda}\left(2\sin\frac{Q_x\Lambda}{4} - \sin\frac{Q_x\Lambda}{2}\right) - \frac{v^2}{8\Lambda}\left(\cos\frac{Q_x\Lambda}{4} - \frac{4}{Q_x\Lambda}\sin\frac{Q_x\Lambda}{4}\right)^2 \tag{4.21}$$

The first term is independent of interparticle interactions. It reflects the cost of nonuniform arrangement of electrons in the periodic external field, as we have seen in (2.49), and will not be important for the subsequent discussion. The second term is the energy gain due to adjustment of the stripes to the external potential and is quadratic in the amplitude of the potential.

When the period of the external potential is about $27/20\Lambda$, ϵ_3 determines the minimal value of the cohesive energy. The interaction dependent part of the energy gain is still given by:

$$-\frac{v^2}{8\Lambda}\left(\cos\frac{Q_x\Lambda}{4}-\frac{4}{Q_x\Lambda}\sin\frac{Q_x\Lambda}{4}\right)^2$$

4.2.2 Long Wavelength Limit, Maximal Energy Gain.

The lowest value of the cohesive energy

$$\epsilon=\epsilon_0-\frac{v^2}{8\Lambda}$$

is achieved at $Q_x\Lambda/4=\pi/2$, i.e. when the period of the external modulation is an even fraction of the stripe period Λ.

In the long wavelength limit ($Q_x\Lambda\ll 1$) the value of the cohesive energy takes on the form:

$$\epsilon=\epsilon_0-\frac{v^2}{72\Lambda}\left(\frac{Q_x\Lambda}{4}\right)^4 \qquad (4.22)$$

The Q_x^4 dependance in the last term is in agreement with the long-wavelength theory of [16].

4.2.3 Displacement of the Edges of the Stripes.

Having determined the energy of the deformed stripes we are now in the position to find the resulting displacements of the edges of the stripes. The derivatives of solutions (4.9) corresponding to the minimal cohesive energy (4.20) are:

$$f'(x) = \epsilon - \epsilon_0 - \frac{v}{2}\cos\frac{Q_x.\Lambda}{4}\cos Q_x.\Lambda x - \frac{2v}{Q_x.\Lambda}\sin\frac{Q_x.\Lambda}{2} =$$
$$\pm\left[(\epsilon - \epsilon_0 + \frac{v}{Q_x.\Lambda}\sin\frac{Q_x.\Lambda}{2})v\cos\frac{Q_x.\Lambda}{4}(1-\cos Q_x.\Lambda x)+\right.$$
$$\left.+\frac{v^2}{4}\cos^2\frac{Q_x.\Lambda}{4}(\cos^2 Q_x.\Lambda x - 1) + \frac{4v}{Q_x}\sin\frac{Q_x.\Lambda}{4}(1-\cos Q_x.\Lambda x)\right]^{\frac{1}{2}} \quad (4.23)$$

We can now construct continuous solutions of (4.9) corresponding to the minimal value of the cohesive energy (4.20). We introduce the amplitude of resulting stripe modulations l_0.

$$l_0 = \frac{2}{Q_x.\Lambda}\sqrt{\frac{8v}{Q_x}\sin\frac{Q_x.\Lambda}{4}}$$

and restore the discrete variable n. Then, to order $\sqrt{v}$, we have:

$$\Lambda_{2n} = \left(n - \frac{1}{4}\right)\Lambda + l_0(1 - \cos\frac{Q_x.\Lambda}{2}n) \quad (4.24)$$

$$\Lambda_{2n+1} = \left(n + \frac{1}{4}\right)\Lambda + l_0\left(1 - \cos\frac{Q_x.\Lambda}{2}\left(n + \frac{1}{2}\right)\right) \quad (4.25)$$

for left and right edges respectively. We have set the shift of the left edge of the zeroth stripe to zero by the choice of the integration constant.

These solutions describe modulations of the stripe positions. In the case of the external period equal to the integer (commensurate periods) and half-integer multiples of the natural period Λ, these modulations are periodic.

For the stripe modulations to be measurable, the fluctuations of the edges should be much less than the amplitude of the calculated shifts. The fluctuations of the stripe edges have been estimated in [12] to be of the order of $\sim \ell$. Therefore, these shifts will have observable consequences if

$$l_0 \gg \ell \tag{4.26}$$

This condition translates into upper bound for the amplitude of the periodic potential:

$$V_0 \gg \frac{\hbar\omega_c}{10(2N-1)} \tag{4.27}$$

While this condition is not satisfied by the experiment described in Sec. 4.1, it can be achieved in the further experiments proposed in [23].

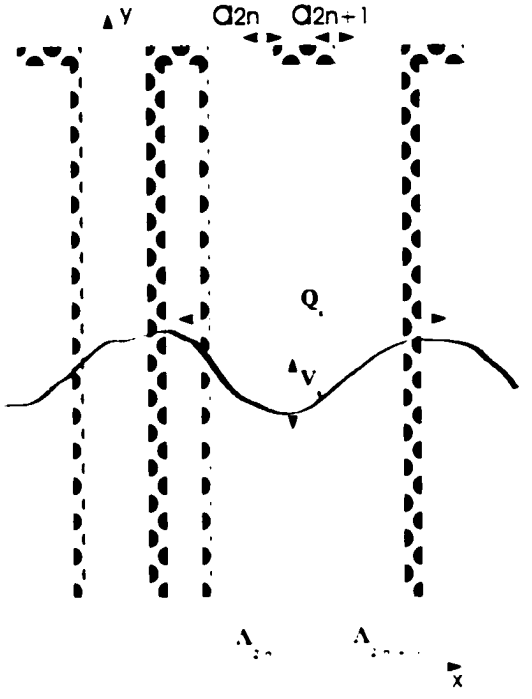

Figure 4.3: Geometry of stripes adjusting to the perpendicular modulation. The modified stripes are shown in grey. For comparison the uniform stripes are shown in black and have been vertically offset for clarity. Left edge of the n^{th} stripe shifts by a_{2n}, right edge - by a_{2n+1}. The applied external modulation is in the $\hat{x}$ direction.

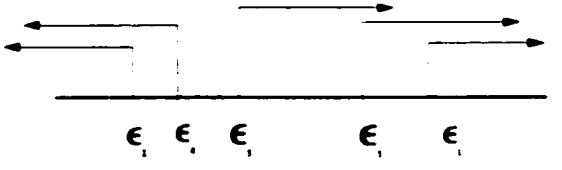

Figure 4.4: Conditions that determine minimal cohesive energy.

4.3 Stripes Aligned Parallel to the Periodic Modulation.

We now consider a different arrangement of the external potential with respect to the stripes: the direction of the modulation will be taken to be along the direction of the stripes, i.e. in the $\hat{y}$ direction as shown on Figure 4.5.

Each stripe can now take advantage of the periodic potential by modulating its density along the applied potential. This requires mixing in contributions to the order parameter with wavevectors proportional to Q_y, the wavevector of the external potential. Any variation in density increases Hartree-Fock interaction energy between the stripes. Hartree-Fock energies of any two density modulations with different wavevectors are separated by a gap of the order u_0, $u_0 \gg V_0$.

As usual for the perturbation theory, higher level contributions to the density are to the lowest order linear in the amplitude of the perturbation. For the simplest periodic potential we are considering, $V(y) = V_0 \cos Q_y y$, only density modulated by the wavevector Q_x will couple to the perturbation. Then we will find that stripes can further minimize the cohesive energy by adjusting their width.

In this section I will use the notation Λ for the width of a stripe anticipating the need to take into account the width change, i.e. $\Lambda = \Lambda - \delta\Lambda$, where $\delta\Lambda$ is the width

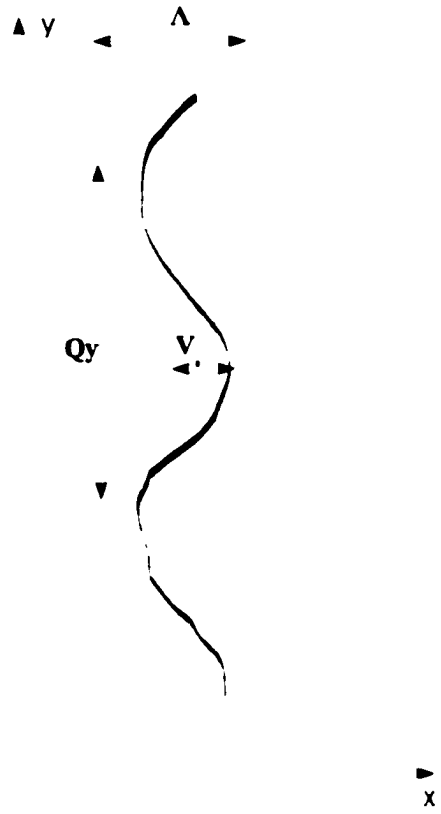

Figure 4.5: Geometry of stripes aligned parallel to the modulation with wavevector Q_y and amplitude V_0.

change. The plan of this section is, therefore, as follows:

- To write down the new order parameter by taking into account that the stripe will be nonuniform in the $\hat{y}$ direction.
- Calculate the cohesive energy with an arbitrary stripe width.
- Find the optimal value of the stripe width.

4.3.1 The Order Parameter and the Cohesive Energy.

To take into the account the contribution to the density of the stripes with wavevector Q_y we make the following ansatz for the expectations of the occupation numbers :

$$\langle a^{\dagger}_{X_-} a_{X_-} \rangle = \delta(q_y) + \xi(\delta(q_y - Q_y) + \delta(q_y + Q_y)), \text{ for } (n - 1/4)\lambda < X < (n + 1/4)\lambda,$$

where ξ is a constant to be determined variationally. Our order parameter (3.11) takes on the form:

$$\tilde{\Delta}(q_x, q_y) = \frac{2}{\lambda q_x} \sin\left(\frac{\lambda q_x}{4}\right) [\delta(q_y) + \xi(\delta(q_y - Q_y) + \delta(q_y + Q_y))]$$

In the real space the expression for the order parameter is:

$$\Delta(x, y) = \frac{1}{L_x L_y} \Theta(\frac{\lambda}{4} - |x|)\{1 - \xi \cos(Q_y y)\} \tag{4.28}$$

The average of the order parameter over the sample should be equal to $1/2L_xL_y$, which requires some caution at $Q_y \to 0$ when the periodic potential becomes a constant. This requirement leads to the following:

$$\Delta(x, y) = \frac{1}{L_x L_y} \Theta(\frac{\lambda}{4} - |x|)\{1 - \xi \frac{\sin(Q_y L_y)}{Q_y L_y} - \xi \cos(Q_y y)\} \tag{4.29}$$

However, our main interest is the experimentally relevant situation of moderate wavevectors, $1/L_y \ll Q_y \lesssim 1/R_c$, and the correction term will unnecessarily clutter the equations. Therefore, I will use the expression (4.28) below that is valid

for any $Q_y = 2\pi n/L_y$ and will relegate the details relevant to $Q_y \to 0$ limit to the Appendix D.

In effect, at any finite Q_y, the density of the stripe is now made up of two components:

$$\rho(x,y) \sim (1-\xi)\Theta(\frac{\lambda}{4} - |x|) + 2\xi V_0 F(Q_y)\Theta(\frac{\lambda}{4} - |x|)\cos^2\left(\frac{Q_y y}{2}\right). \tag{4.30}$$

where the first term is the contribution to the total density of the uniform component and the second is the contribution of the nonuniform one.

The expression for the cohesive energy transformed to the real space is, as before (4.3):

$$E_{coh} = \frac{1}{2\bar{\nu}}\int dx dy\,(e(x,y) + V_0 F(Q_y)\cos(Q_y y))\left(\Delta(x,y) - \frac{\bar{\nu}}{L_x L_y}\right). \tag{4.31}$$

where we have introduced the potential

$$e(x,y) = n_L L_x L_y \int dx' dy' u_{HF}^{eff}(x-x', y-y')\Delta(x',y') \tag{4.32}$$

The external potential energy contribution is easily evaluated to be:

$$\begin{aligned}&\frac{1}{2\bar{\nu}}\int dx dy V_0 F(Q_y)\cos(Q_y y)\Theta(\frac{\lambda}{4} - x')(1-\xi\cos(Q_y y) = \\ &= \xi\frac{V_0 F(Q_y)}{2\bar{\nu}}\int dx\Theta(\frac{\lambda}{4} - x')\int dy\cos^2(Q_y y) = \xi\frac{V_0 F(Q_y)}{8\bar{\nu}}\end{aligned} \tag{4.33}$$

where the notations are the same as before: $v = V_0 F(Q_y)/u_0$ as in (4.6) except for Q_y replacing Q_x.

It is essential that the nonuniform components of the stripes now interact with the full two dimensional potential (3.15), in contrast with the their uniform components whose interaction is still described by (3.20).

To calculate $e(x,y)$ we Fourier transform (3.15), and obtain [74]:

$$\int \frac{dq_x}{2\pi} e^{iq_x(x-x')} \frac{\sin(2R_c\sqrt{q_x^2+Q_y^2})}{2R_c\sqrt{q_x^2+Q_y^2}} = \frac{1}{2} J_0\left(Q_y\sqrt{4R_c^2-(x-x')^2}\right)\Theta(2R_c-|x-x'|) \tag{4.34}$$

This is the effective interaction of two stripes modulated by the wavevector Q_y in the y direction. Therefore

$$e(x,y) = \int dx' u_0 \Theta(2R_c - |x-x'|) \times \left[\left(1+\xi J_0\left(Q_y\sqrt{4R_c^2-(x-x')^2}\right)\cos Q_y y\right)\Theta\left(\frac{\lambda}{4}-|x'|\right)-\bar{\nu}\right] \tag{4.35}$$

To obtain the cohesive energy, I perform the integration in Eq. (4.31). The integral involved is a particular case of the integral described in the Appendix C for $f(x) = J_0\left(Q_y\sqrt{4R_c^2-x^2}\right)$. All but one of the remaining integrals can be done using the following tabulated integrals [74]:

$$\int du\, u J_0(Qu) = \frac{u J_1(Qu)}{Q}$$

$$\int_0^z du J_0(\sqrt{z^2-u^2}) = \sin z$$

Then, adding the external potential contribution (4.33), I get the following expression

for the cohesive energy:

$$\epsilon = \left[\frac{\lambda^2}{2} - 3\lambda R_c - 4R_c^2 + \frac{\xi^2}{2Q_y}\left(4\sqrt{4R_c^2 - \frac{\lambda^2}{4}}J_1\left(Q_y\sqrt{4R_c^2 - \frac{\lambda^2}{4}}\right) - \right.\right. \tag{4.36}$$

$$\left.\left. -4R_cJ_1(2Q_yR_c) - \lambda\sin(2Q_yR_c) + 2\lambda Q_y\int_0^{\lambda/2} du J_0(Q_y\sqrt{4R_c^2 - u^2})\right)\right]/\lambda + \xi\frac{v}{4}$$

For any value of the period of the stripes λ we can choose the variational parameter that controls higher level contribution ξ which gives the lowest energy. Minimizing this expression of cohesive energy with respect to the variational constant ξ, we find that:

$$\xi_{min} = -\frac{vQ_y\lambda}{4}\left(4\sqrt{4R_c^2 - \frac{\lambda^2}{4}}J_1\left(Q_y\sqrt{4R_c^2 - \frac{\lambda^2}{4}}\right) - 4R_cJ_1(2Q_yR_c) - \right.$$

$$\left. -\lambda\sin(2Q_yR_c) + 2\lambda Q_y\int_0^{\lambda/2} du J_0(Q_y\sqrt{4R_c^2 - u^2})\right)^{-1} \tag{4.37}$$

With this ξ the value of the cohesive energy is:

$$\epsilon = \frac{1}{\lambda}\left[\frac{\lambda^2}{2} - 3\lambda R_c + 4R_c^2\right] - \frac{v^2Q_y\lambda}{32}\left(4\sqrt{4R_c^2 - \frac{\lambda^2}{4}}J_1\left(Q_y\sqrt{4R_c^2 - \frac{\lambda^2}{4}}\right) - \right.$$

$$\left. -4R_cJ_1(2Q_yR_c) - \lambda\sin(2Q_yR_c) + 2\lambda Q_y\int_0^{\lambda/2} du J_0(Q_y\sqrt{4R_c^2 - u^2})\right)^{-1} \tag{4.38}$$

As expected, the first term is the cohesive energy of the uniform stripe (compare (3.23) with λ replacing Λ). The second term is the second order perturbation theory contribution due to level mixing. The denominator in the second term is the difference between Hartree-Fock energies of the uniform and modulated stripes.

The energy gain increases with increasing Q_y, which is easy to understand. Recall that the guiding centers of two wavefunctions with wavevector Q_y are separated by the distance $Q_y \ell^2$. Therefore, at larger Q_y the wavefunctions are separated by a greater distance. This reduces their Hartree-Fock interaction and allows them to take greater advantage of the external potential.

Let us consider the limit of small wavevectors, $1/L_y \ll Q_y \ll 1/R_c$. In this limit the value of the cohesive energy is:

$$\epsilon = \epsilon_0 - \frac{e^2(\sqrt{2}+1)}{64 R_c}\left(1 + \frac{34+25\sqrt{2}}{24} Q_y^2 R_c^2\right) \tag{4.39}$$

4.3.2 Adjusting the Stripe Width.

The modulating potential along the length of the stripes in effect compresses them. This phenomenon will be taken into account below. In principal, the cohesive energy can be further lowered by making the stripes wider, but that correction to the cohesive energy is beyond the validity of the present approximation.

Here I am going to calculate the change in the width of the stripes. Minimizing (4.38) with respect to λ, one obtains the equation that determines the width reduction:

$$\left(\frac{2R_c}{\lambda}\right)^2 - \frac{1}{2} - \frac{e^2 Q_y}{32}\left(\frac{\Xi'(\lambda)\lambda - \Xi(\lambda)}{\Xi^2(\lambda)}\right) = 0. \tag{4.40}$$

where

$$\Xi(\lambda) = 4\sqrt{4R_c^2 - \frac{\lambda^2}{4}}J_1\left(Q_y\sqrt{4R_c^2 - \frac{\lambda^2}{4}}\right) -$$
$$-4R_cJ_1(2Q_yR_c) - \lambda\sin(2Q_yR_c) + 2\lambda Q_y\int_0^{\lambda/2} du J_0(Q_y\sqrt{4R_c^2 - u^2}) \quad (4.41)$$

The derivative of $\Xi(\lambda)$ is:

$$\Xi'(\lambda) = -\frac{\lambda}{\sqrt{4R_c^2 - \frac{\lambda^2}{4}}}J_1\left(Q_y\sqrt{4R_c^2 - \frac{\lambda^2}{4}}\right) + \frac{Q_y\lambda}{2}\left\{J_0\left(Q_y\sqrt{4R_c^2 - \frac{\lambda^2}{4}}\right) +\right.$$
$$\left. - J_2\left(Q_y\sqrt{4R_c^2 - \frac{\lambda^2}{4}}\right)\right\} - \sin 2Q_yR_c + 2Q_y\int_0^{\lambda/2} du J_0(Q_y\sqrt{4R_c^2 - u^2}) \quad (4.42)$$

Recalling that $\Lambda = 2\sqrt{2}R_c$, I find from (4.40) that the change in width of the stripes, $\delta\Lambda = \lambda - \Lambda$, to the lowest order in v, is determined by:

$$2\left(\frac{2R_c}{\Lambda}\right)^2\frac{\delta\Lambda}{\Lambda} - \frac{v^2Q_y}{32}\frac{\Xi'(\Lambda).\Lambda - \Xi(\Lambda)}{\Xi^2(\Lambda)} = 0. \quad (4.43)$$

Therefore $\delta\Lambda$ is:

$$\delta\Lambda = \Lambda\frac{v^2Q_y}{32}\frac{\Xi'(\Lambda).\Lambda - \Xi(\Lambda)}{\Xi^2(\Lambda)} \quad (4.44)$$

With the help of the Bessel function recurrence formula [74]:

$$zJ_{\beta-1}(z) + zJ_{\beta+1}(z) = 2\beta J_\beta(z)$$

the expression (4.42) for $\Xi'(\Lambda)$ at $\Lambda = 2\sqrt{2}R_c$ can be simplified to yield:

$$\Xi'(\Lambda) = -\sin(2Q_yR_c) + 2Q_y\int_0^{\Lambda/2} du J_0(Q_y\sqrt{4R_c^2 - u^2}).$$

whereas

$$\Xi(\Lambda) = 2\Lambda J_1\left(\frac{Q_y\Lambda}{2}\right) - 4R_c J_1(2Q_y R_c) - \Lambda\sin(2Q_y R_c) - 2Q_y\Lambda\int_0^{\Lambda/2} du J_0(Q_y\sqrt{4R_c^2 - u^2})$$

Finally, the expression for the change in the stripe width takes the form:

$$\delta\Lambda = \Lambda\frac{v^2 Q_y}{32}\times \tag{4.45}$$
$$\frac{2\Lambda\sin(2Q_y R_c) + 4R_c J_1(2Q_y R_c) - 2\Lambda J_1\left(\frac{Q_y\Lambda}{2}\right)}{(2\Lambda J_1\left(\frac{Q_y\Lambda}{2}\right) - 4R_c J_1(2Q_y R_c) - \Lambda\sin(2Q_y R_c) - 2Q_y\Lambda\int_0^{\Lambda/2} du J_0(Q_y\sqrt{4R_c^2 - u^2}))^2}$$

The width reduction is a monotonically increasing function of Q_y. At small wavevectors, $1/L_y \ll Q_y \ll 1/R_c$,

$$\delta\Lambda = \frac{v^2}{32(3-\sqrt{2})R_c}\left(1 + \frac{7}{24}(Q_y R_c)^2\right)$$

Therefore, alignment of the stripes parallel to the potential increases the width of the stripes. This increase is second order in $V_0/\hbar\omega_c$ and would give fourth order correction to the cohesive energy, which is beyond the validity of the present approximation.

4.4 Energy Comparison: Parallel or Perpendicular Alignment?

We can now compare this value with the corresponding expression in the perpendicular alignment (4.20). On Fig. 4.6 we plot energy gain due to the periodic potential in both configurations. Parallel alignment can be seen to have lower cohesive energy at all wavevectors. In the numerical simulations of Yoshioka [27] parallel alignment was also found to have lower cohesive energy for all ($2 \leq m \leq 6$) ratios of periods studied. This indicates that shifting the stripes and changing their width (the channel of energy reduction in the perpendicular alignment) is less effective than the introduction of a nonuniform component while keeping the same stripe width (the channel of energy reduction in the parallel alignment). At long wavelengths, each stripe in the perpendicular alignment effectively experiences a constant potential and has to shift as a whole. This turns out to be energetically more expensive than the introduction of a nonuniformity. At shorter wavelengths, the cost of creating the nonuniform density component is even smaller since the electrons creating it are separated by a greater distance and their Hartree-Fock interaction is reduced.

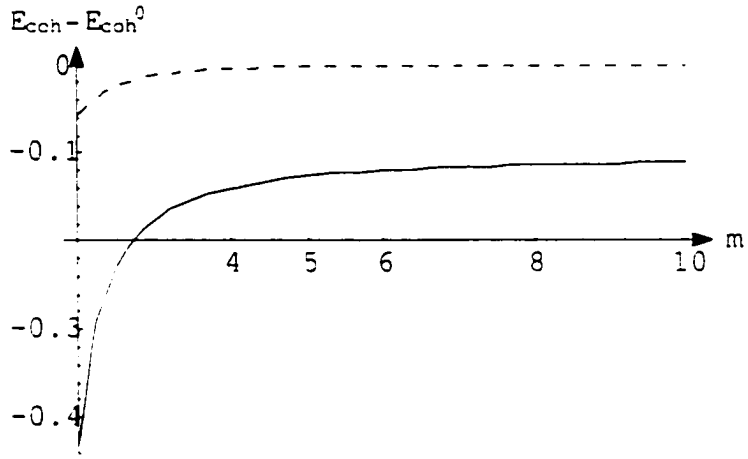

Figure 4.6: Comparison of energy gain due to the periodic potential in two configurations. Dashed line is for the perpendicularly aligned stripes: solid line - for parallel alignment. Vertical axis is in units v^2/Λ. Along the x axis we plot the ratio of the period of the potential to the stripe period, i.e. $m = 2\pi/Q\Lambda$.

4.5 Conductivity Across the Modulated Stripes in a Perpendicular Alignment.

To study transport in the modulated stripes we adopt the Boltzmann transport equation in the constant relaxation time approximation approach developed by Macdonald and Fisher in [16] for the case of uniform stripes.

Recall that the stripes in the partially filled Landau level ($\bar{\nu} = \frac{1}{2}$) are separated by the electron liquid of the filled lower Landau level. We will refer to these as hole stripes, as is often done in the literature.

In the approach of [16], collective sliding motion of the charge density wave is assumed to be absent and the electrical transport at $T = 0$ is dominated by single-particle interedge tunnelling of electrons across the hole stripes. The tunnelling current is determined by:

- the potential drop across the hole stripes
- the scattering times across the electron and hole stripes
- the charge per unit energy at the tunnelling edge.

The variation of the width of electron and hole stripes in the periodic potential has two consequences. The change in the width of hole stripes changes the potential drop

across them. It also changes the charge per unit energy at the edges.

The constant tunnelling times (denoted below as τ_e and τ_h, for tunnelling across electron and hole stripes respectively) are determined by the impurity scattering rates and are not modified by the widths' modulations. In principle, for the electron gas in a quantizing magnetic field the assumption of a constant tunnelling time can be improved by self-consistently taking into account the collision broadening of Landau levels. This can be achieved, for instance, in the self-consistent Born approximation. In ref. [4] this program has been implemented for a homogeneous electron gas in a one-dimensional periodic potential.

I will determine the tunnelling current across the n^{th} stripe by calculating the change in the chemical potential drop across it due to the shift in the position of the edges. Then, for some values of the period of the external potential, I will be able to pick a stripe whose width remains unchanged with respect to the unperturbed case. Calculating the current through this stripe determines the total steady state current in the hard direction - perpendicular to the stripes, in this case the stripes can be thought of as connected in parallel due to current conservation.

Let us choose the axes so the direction $\hat{x}$ is perpendicular to the stripes, as shown on the Fig. 4.7. If I take the zero of the chemical potential μ at $x = 0$ (the center of the zeroth stripe at $V_0 = 0$), then for the chemical potential for the electrons on

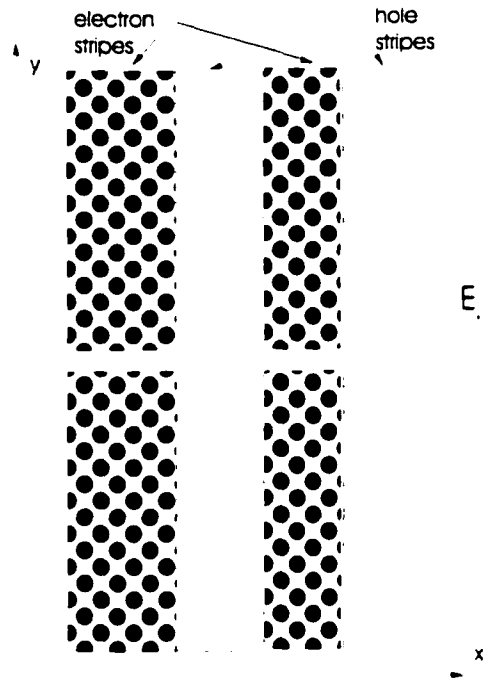

Figure 4.7: Illustration of the stripe state in the electric field. The state can be viewed as consisting of alternating electron and hole stripes. The stripes with dark circles, representing cyclotron orbits, are electron stripes in the partially filled Landau level. The stripe with the gray-colored cyclotron orbits are hole stripes.

the left and right edges of the n^{th} stripe we have (recall our parameterization of the stripe positions (4.8)):

$$\mu_{2n} = eE_x\left(n\Lambda + \frac{a_{2n} + a_{2n+1}}{2}\right) - \frac{\mu}{2} \text{ and } \mu_{2n+1} = eE_x\left(n\Lambda + \frac{a_{2n} + a_{2n+1}}{2}\right) + \frac{\mu}{2},$$

where the electric field is applied in the $\hat{x}$ direction. The chemical potential change

across the n^{th} electron stripe and the adjacent hole stripe on the left are

$$\mu_{2n-1} - \mu_{2n} = \mu \text{ and } \mu_{2n} - \mu_{2n-1} = eE_x(n\Lambda + \frac{1}{2}(a_{2n} + a_{2n+1} - a_{2n-1} - a_{2n-2})) - \mu$$

The change in the chemical potential is due to the tunnelling of electrons across the electron and hole stripes:

$$\dot{\mu}_{2n-1} = \frac{\mu_{2n} - \mu_{2n-1}}{\tau_e} + \frac{\mu_{2n+2} - \mu_{2n+1}}{\tau_h} \text{ and } \dot{\mu}_{2n} = \frac{\mu_{2n-1} - \mu_{2n}}{\tau_e} + \frac{\mu_{2n-1} - \mu_{2n}}{\tau_h}.$$

Eliminating the chemical potentials at the edges in favor of μ and taking into account that in the steady state $\dot{\mu}_{2n}$ (as well as $\dot{\mu}_{2n-1}$) is equal to zero, allows us to determine the steady state chemical potential:

$$\mu\left(\frac{1}{\tau_e} + \frac{1}{\tau_h}\right) = eE_x \frac{\Lambda + \frac{1}{2}(a_{2n+1} + a_{2n} - a_{2n-1} - a_{2n-2})}{\tau_h} \tag{4.46}$$

The current across the hole stripe to left of the n^{th} electron stripe is then given by:

$$I_x(n) = \frac{eL_y}{hv_F(n)} \frac{\mu_{2n} - \mu_{2n-1}}{\tau_h} =$$
$$= \frac{eL_y}{hv_F(n)} eE_x \left(\Lambda + \frac{a_{2n-1} + a_{2n} - a_{2n-1} - a_{2n-2}}{2}\right) \cdot (\tau_e - \tau_h). \tag{4.47}$$

where $eL_y/hv_F(n)$ is the charge per unit energy and $v_F(n)$ is "Fermi velocity" of the electrons on the tunnelling edge of the n^{th} stripe. The second term in parenthesis is the correction to the current due to the shift of stripe edges.

To understand the change in Fermi velocity, we recall that each stripe can be thought of as a quantum Hall droplet with chiral quasi-particles propagating along

its left and right edges. The quasi-particle momentum is proportional to the guiding center coordinate. Therefore, increasing (decreasing) the width of a stripe creates the states with higher (lower) momentum.

To compare the conductivity in the perturbed system with that of the pure charge density wave with the period Λ as calculated in [16], we will identify and consider the stripe whose width remains unchanged with respect to the $\epsilon = 0$ case, i.e. $a_{2n+1} - a_{2n} = 0$. This will ensure that particles tunnelling from such a stripe will do so with unaltered Fermi velocity. As the stripes are "connected in parallel", current through this stripe determines the steady state current through the system.

In Sec. 4.2.3 I have obtained the displacements of the edges of the stripes. Recall that in Eq. (4.24) shifted positions of the n^{th} stripe have been calculated to be:

$$\Lambda_{2n} = \left(n - \frac{1}{4}\right)\Lambda + l_0(1 - \cos\frac{Q_x\Lambda}{2}n)$$
$$\Lambda_{2n+1} = \left(n + \frac{1}{4}\right)\Lambda + l_0\left(1 - \cos\frac{Q_x\Lambda}{2}\left(n + \frac{1}{2}\right)\right)$$

Therefore the width of the n^{th} stripe, $\Lambda_{2n+1} - \Lambda_{2n}$ is unchanged if

$$\cos\frac{Q_x\Lambda}{2}n - \cos\frac{Q_x\Lambda}{2}\left(n - \frac{1}{2}\right) = 0.$$

which leads to the following condition on the ratio of the period of the external potential $b = 2\pi/Q_x$ and the period of the charge density wave. If

$$\frac{b}{\Lambda} = \frac{4p+1}{2s} \tag{4.48}$$

for some integer positive integers p and s, the width of the p^{th} stripe will not change.

If this condition is satisfied, the current (4.47) across the hole stripe adjacent to this electron stripe is given by ($v_F(k) = v_F$):

$$I_x(k) = \frac{eL_y}{hv_F} eE_x \left(\Lambda - (-1)^s 2l_0 \sin^2 \frac{Q_x \Lambda}{2} \cos \frac{Q_x \Lambda}{4} \right) \frac{1}{\tau_e + \tau_h}$$

Finally we obtain an expression for the fractional change in the conductivity free of phenomenological parameters:

$$\begin{aligned} \frac{\Delta\sigma_{xx}(v)}{\sigma_{xx}(0)} &= (-1)^{s-1} \frac{2l_0}{\Lambda} \sin^2 \frac{Q_x \Lambda}{2} \cos \frac{Q_x \Lambda}{4} = \\ &= (-1)^{s-1} \frac{4}{Q_x \Lambda^2} \sqrt{\frac{8v}{Q_x} \sin \frac{Q_x \Lambda}{4}} \sin^2 \frac{Q_x \Lambda}{2} \cos \frac{Q_x \Lambda}{4} \end{aligned} \tag{4.49}$$

Two things are worth noticing about this result. First of all, the sign of the correction to the conductivity is very sensitive to the relationship between the periods of stripes and external potential. Secondly, it is proportional to the square root of the small amplitude of the potential.

Let us return to the period matching conditions (4.48) that determine the existence of a stripe with an unaltered width and the sign of the correction to the conductivity (4.49) and examine them in a more detail. The sign of the correction to the conductivity depends on the parity of s and the sign of

$$\cos \frac{Q_x \Lambda}{4} = \cos \frac{\pi s}{4p + 1}$$

For instance, if $2s < 4p+1$ and and s is even, then the correction to the conductivity is *negative*, while it is *positive* for s - odd.

If $4p + 1 > s > (4p + 1)/2$, the situation is reversed and the correction to the conductivity is *positive* for s even and *negative* for odd s.

This result has very clear experimental consequences, provided the condition on the value of the amplitude of the external potential (4.27) is satisfied. One and the same sample should be fabricated into several sequential Hall bars. This would insure that scattering times don't change from sample to sample as is implied by Eq. (4.47). One the bars is left as a reference (as is conventionally done [23]) and other processed into lateral superlattices of different periods, with periods satisfying conditions (4.48). Assuming that superlattice preparation does not significantly modify the distribution of impurities, the fractional change of conductivity in the processed samples with respect to the reference should show the behavior predicted by Eq. (4.47) and discussed above.

4.6 Conclusions.

In summary, we have calculated the cohesive energy in the limit of small amplitude and arbitrary period of the external potential for two cases: when the stripes are

aligned perpendicular and when they are aligned parallel to the direction of an external periodic modulation.

In the former case the external potential changes widths of the stripes as well as displaces centers of the stripes. Both of these effects have been taken into account by considering stripes' edges as dynamical variables. The resulting shifts of the edges are nonanalytic in the amplitude of the external potential.

In the latter case only the width of the stripes can change, whereas the positions of the centers of the stripes remain unmodified by the perturbation.

In both cases we find a decrease in the cohesive energy proportional to the square of the amplitude in agreement with numerical simulations [27], [25].

We find that alignment parallel to the direction of the external modulation has lower cohesive energy for all periods of the external potential. Therefore the parallel alignment should be always realized, once the native anisotropy barrier [26] has been overcome.

There is an experimental prediction that follows from our analysis of the corrections to the conductivity in the perpendicular to the stripes direction. This correction is very sensitive to the ratio of the period of the external potential to the natural period of the stripes. The correction to the conductivity can be either positive or negative depending on the value of the ratio.

Part II

Current Correlators

in the Calogero-Sutherland Model.

4.7 Introduction to the Calogero-Sutherland Model.

Even though current emphasis in the physics of the Quantum Hall systems has shifted towards the understanding of the behavior in weak magnetic fields as described in Part I. the original Fractional Quantum Effect has not yielded to a full microscopic description. Despite all the success of the composite fermion description a microscopic mechanism of anyon creation is lacking.

How do the interactions of of the electrons in the strong magnetic field with a given one conspire to behave as an additional magnetic field? The exactly solvable Calogero-Sutherland model of interacting particles with the inverse square interaction potential discussed below provides an explicit, albeit one-dimensional, example of how this may happen. The result is a model of one-dimensional anyons as will be illustrated in Sec. 5.

Due to the fact that the ground state wavefunction of the model is a one-dimensional version of a Laughlin wavefunction describing the ground state in the fractional quantum Hall effect, the construction of excitations in the Calogero-Sutherland model provides a direct analog to the corresponding construction in the fractional quantum Hall case. The excitations on the boundary of the fractional quantum Hall incompressible droplet, so called edge excitations, can be described by the symmetric polynomials as has been first demonstrated by M. Stone [48] following [37].

There has been a lot of progress in understanding this particular one-dimensional system. The accumulated knowledge about it includes exact results on the dynamical density-density correlation function [40, 41], advanced [42] and retarded [40] Green's functions. The most general method available for the computation of the correlation functions involves the implementation of Jack polynomials, introduced in 5.1.

In this part of this work I extend the method of Jack polynomials [40, 41, 46] to the calculation of the exact dynamical polarization tensor [47]. I begin by discussing the eigenstates of the model in Sec. 5. The further development requires a review of properties of Jack polynomial and partitions. This is done in Sec. 5.1. The elucidate the quasiparticle content of correlation functions calculated in Sec. 6. I review the notion of fractional exclusion statistics in Sec. 5.2.

Glossary.

The notations used in Part II of this work are collected below.

Partition:

$$\boldsymbol{\kappa} = (\kappa_1, \kappa_2, \ldots, \kappa_N).$$

Conjugate partition:

$$\boldsymbol{\kappa}' = (\kappa'_1, \kappa'_2, \ldots, \kappa'_N)$$

Arm-length:

$$a(s) = \kappa_i - j$$

Arm-colength:

$$a'(s) = j - 1$$

Leg-length:

$$l(s) = \kappa'_j - i$$

Leg-colength:

$$l'(s) = i - 1$$

Upper hook-lengths:

$$h^{\bullet}_{\kappa}(s) = l(s) + \frac{1 + a(s)}{\lambda}$$

Lower hook-lengths:

$$h^{\kappa}_{\bullet}(s) = l(s) + 1 + \frac{a(s)}{\lambda}$$

Chapter 5

Eigenstates of Calogero-Sutherland Model

The Calogero-Sutherland model describes the dynamics of spinless particles with inverse-square interactions on a ring with the circumference L. In this section I introduce the Calogero-Sutherland model and show how to construct the general eigenstates of the model following Sutherland [33]. The Hamiltonian for the Calogero-Sutherland model of N particles is given by:

$$H_N^{\mathrm{CS}} = \sum_i^N \frac{p_i^2}{2m} + \frac{\hbar}{m}\left(\frac{2\pi}{L}\right)^2 \sum_{i<j} \frac{\lambda(\lambda-1)}{\sin^2 \frac{\pi}{L}(x_i - x_j)} \tag{5.1}$$

In the following I will take $\frac{\hbar}{2m} = 1$ and restrict the discussion to the rational values of the coupling constant $\lambda = p/q$.

The ground state wavefunctions of the model at integer values of λ correspond to 1D versions of Laughlin's wavefunctions [36] and are given by

$$\Psi_0 = \prod_{i<j}(z_i - z_j)^\lambda \prod_k z_k^{J_0}. \tag{5.2}$$

where the current $J_0 = -\lambda(N-1)/2$ and

$$z_j = \exp(i2\pi x_j/L) \tag{5.3}$$

When $0 < \lambda < 1$ there is another possible ground state with power $1-\lambda$: however, only the solution with power λ will be considered for reasons of continuity with $\lambda > 1$ solutions.

The excited states of this model are constructed by multiplying the ground state wavefunction by some symmetric polynomials, and this construction is analogous to that of the gapless edge excitations of the quantum Hall effect [37]. A general excited state $\Psi^\lambda_{\boldsymbol{\kappa}} = \Psi_0 J^{1,\lambda}_{\boldsymbol{\kappa}}$ is labelled by the quantum numbers $\boldsymbol{\kappa} = (\kappa_1, \kappa_2, \ldots, \kappa_N)$, and $J^{1,\lambda}_{\boldsymbol{\kappa}}$ satisfies the following new eigenvalue equation

$$H J^{1/\lambda}_{\boldsymbol{\kappa}} = E_{\boldsymbol{\kappa}} J^{1/\lambda}_{\boldsymbol{\kappa}}. \tag{5.4}$$

where

$$H = \sum_{j=1}^{N}(z_j\partial_{z_j})^2 + \lambda \sum_{j<k} \frac{z_j + z_k}{z_j - z_k}(z_j\partial_{z_j} - z_k\partial_{z_k}). \tag{5.5}$$

The eigenenergy $E_{\boldsymbol{\kappa}}$ is given by

$$E_{\boldsymbol{\kappa}} = \left(\frac{2\pi}{L}\right)^2 \sum_{i}^{N} (\kappa_i^2 + \lambda(N + 1 - 2i)\kappa_i) \tag{5.6}$$

This energy eigenvalue plus the ground state energy can be rewritten in terms of newly defined pseudomomenta k_j as

$$E_{\boldsymbol{k}} = \frac{\hbar^2}{2m} \sum_{j=1}^{N} k_j^2. \tag{5.7}$$

where

$$Lk_j = 2\pi I_j + \pi(\lambda - 1) \sum_{l=1}^{N} \mathrm{sgn}(k_j - k_l). \tag{5.8}$$

The quantum numbers I_j are now distinct (half-odd) integers and are related to κ_j's by $I_j = \kappa_j + (N + 1 - 2j)/2$.

Actually, the hamiltonian of the model can be rewritten to reflect this structure of quantum numbers. Polychronakos [38] showed by introducing

$$\pi_j = p_j + i\pi\lambda/L \sum_{i \neq j} \cot(\pi(x_i - x_j)/L) P_{ij}. \tag{5.9}$$

where p_j is the ordinary momentum operator, the Hamiltonian

$$H = \sum_j \pi_j^2$$

is fully integrable and is the same as the Calogero-Sutherland model up to a modification $\lambda(\lambda - P_{ij})$ plus some trivial constant. The new operator π_j is the momentum operator for the pseudo-particles, and the momenta $\sum_j k_j$ corresponds to the

eigenvalues of $\sum_j \pi_j$. This new Hamiltonian should be considered as the model of one-dimensional "anyons" with fractional exchange statistics [38].

The distribution of k_j determined by Eq. (5.8) is used to construct pictorial representations of the eigenstates which are useful for exposing the fractional statistics obeyed by the elementary excitations of the model.

In general, the eigenstates of the Hamiltonian H can be represented in terms of the following bosonic basis states:

$$\Phi(\kappa) = \sum_P \prod_{j=1}^{N} z_j^{\kappa_P}. \tag{5.10}$$

where the sum extends over all permutations of the integer set κ which can be considered as a set of bosonic quantum numbers with no restrictions on their values. Since $\Phi(\kappa)$ does not depend on the ordering of the quantum numbers, let $\kappa_1 \geq \kappa_2 \geq \ldots \geq \kappa_N$ without loss of generality. These symmetric polynomials form a complete basis.

5.1 Jack Symmetric Polynomials

The polynomial solutions of Eq. (5.4) in Section 5 are also known in the mathematical literature as Jack polynomials [57]. In fact, Stanley [58] has shown that the complete set of linearly independent solutions of Eq. (5.4) is indeed given by Jack polynomials

up to global translation (i.e., up to the factor $\prod_{j=1}^{N} z_j^J$ where J is the current and takes an arbitrary real number) [40].

This section is divided into two subsections: the first introduces the conventional notations used in mathematical literature and the second some of the general properties of Jack polynomials.

5.1.1 Introduction to Notations of Partitions.

Partitions are defined as sequences of non-negative integers in non-increasing order and are used to label the symmetric polynomials. They are denoted by bold-face Greek letters as

$$\boldsymbol{\kappa} = (\kappa_1, \kappa_2, \ldots, \kappa_N). \tag{5.11}$$

where $\kappa_1 \geq \kappa_2 \geq \ldots \geq \kappa_N$. Non-zero κ_j are called *parts* of $\boldsymbol{\kappa}$ whose *length* (i.e., the total number of non-zero *parts*) is denoted by $\ell(\boldsymbol{\kappa})$. The *weight* of the partition is defined by $|\boldsymbol{\kappa}| = \sum_{j=1}^{\ell(\boldsymbol{\kappa})} \kappa_j$. If $\kappa_1 + \ldots + \kappa_i \geq \mu_1 + \ldots + \mu_i$ for all $i \geq 1$, then $\boldsymbol{\kappa} \geq \boldsymbol{\mu}$.

Young diagram $D(\boldsymbol{\kappa})$ is used to graphically represent a partition: $D(\boldsymbol{\kappa}) = \{(i, j) : 1 \leq i \leq \ell(\boldsymbol{\kappa}),\ 1 \leq j \leq \kappa_i\}$. The cell labelled by (i, j) is situated in the i-th row and the j-th column of the Young diagram. The diagram of $\boldsymbol{\kappa}$, therefore, consists of $\ell(\boldsymbol{\kappa})$ rows of lengths κ_j.

A *conjugate* of $\boldsymbol{\kappa}$ is denoted by $\boldsymbol{\kappa}' = (\kappa_1', \kappa_2', \ldots)$ and corresponds to a partition

whose diagram is obtained by changing all the rows of $\mathcal{D}(\boldsymbol{\kappa})$ to columns in non-increasing order from the left to right. For example, the conjugate of $\boldsymbol{\kappa} = (5,4,4,1)$ shown on Fig. 5.1 is $\boldsymbol{\kappa}' = (4,3,3,3,1)$. Now, the following simple but useful identity can be derived [59]

$$n(\boldsymbol{\kappa}) \equiv \sum_{i=1}^{\ell(\boldsymbol{\kappa})} (i-1)\kappa_i = \sum_{i=1}^{\ell(\boldsymbol{\kappa}')} \binom{\kappa'_i}{2}. \tag{5.12}$$

In order prove Eq. (5.12) every cell in the ith row of $\mathcal{D}(\boldsymbol{\kappa})$ is filled in with an integer $i-1$. Since $n(\boldsymbol{\kappa})$ corresponds to the sum of all the integers in the diagram, the two different expressions for $n(\boldsymbol{\kappa})$ are obtained depending on whether the numbers in each row or column are summed first.

For a given cell $s = (i,j)$ of a diagram $\mathcal{D}(\boldsymbol{\kappa})$ there are corresponding *arm-length*

$$a(s) = \kappa_i - j,$$

arm-colength

$$a'(s) = j - 1,$$

leg-length

$$l(s) = \kappa'_j - i,$$

and *leg-colength*

$$l'(s) = i - 1$$

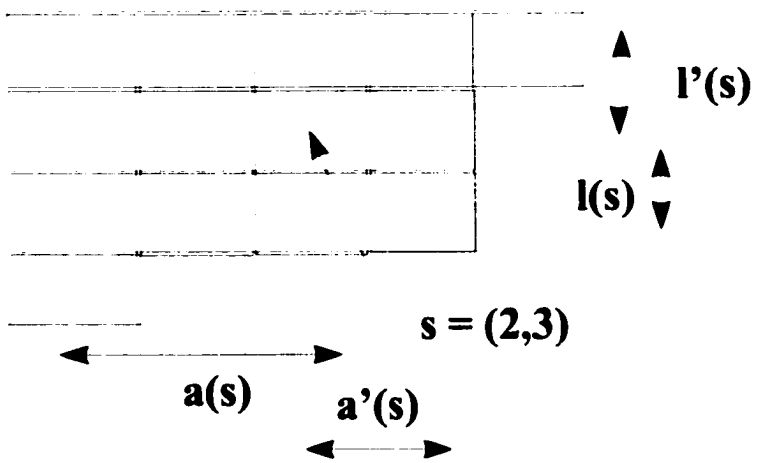

Figure 5.1: Illustration of the Young diagram $\mathcal{D}(\kappa)$ for the partition $\kappa = (5,4,4,1)$.

The *upper* and *lower hook-lengths* are defined, respectively, as

$$h^*_\kappa(s) = l(s) + \frac{1 + a(s)}{\lambda}. \tag{5.13}$$

$$h^\kappa_*(s) = l(s) + 1 + \frac{a(s)}{\lambda}. \tag{5.14}$$

An illustration below shows the partition $(5,4,4,1)$. The arm-length, arm-colength, leg-length, and leg-colength for the cell $s = (2,3)$, i.e the number of cells to the north, south, east, and west, are also shown.

5.1.2 Properties of Jack Symmetric Polynomials.

The symmetric polynomials are indexed by the partitions. The bosonic basis functions $\Phi(\kappa)$ of the Calogero-Sutherland model are called the monomial symmetric functions

and the quantum numbers κ correspond to the partitions defined in the previous subsection. Since the quantum numbers are allowed to be negative integers, the correspondence is only up to some trivial constant translation. This restriction to non-negative integer parts is more of a convenience than a restriction since the Calogero-Sutherland Hamiltonian is invariant under the translation.

Following the established notation convention [58], I shall denote Jack symmetric polynomials as $J_{\boldsymbol{\kappa}}^{1/\lambda}(\{z_i\})$. If $\lambda = 1$, Jack polynomials reduce to Schur functions which describe the excited states of the free fermions [48]. At $\lambda = 0$, it becomes the monomial symmetric function which is just the free bosonic wavefunction. If $\lambda = 2$ or $1/2$, they are called the zonal spherical functions. As $\lambda \to \infty$, $J_{\kappa}^{1/\lambda}$ reduce to the elementary symmetric functions.

One way of defining Jack polynomials is based on the properties of the power-sum symmetric function $p_{\boldsymbol{\kappa}} = p_{\kappa_1} p_{\kappa_2} p_{\kappa_3} \ldots$, where $p_{\kappa_i} = \sum_j z_j^{\kappa_i}$. A scalar product on the vector space of all symmetric functions of finite degree is defined as

$$\langle p_{\boldsymbol{\kappa}}, p_{\boldsymbol{\mu}} \rangle_{1/\lambda} = \delta_{\boldsymbol{\kappa},\boldsymbol{\mu}} z_{\boldsymbol{\kappa}} \lambda^{-\ell(\boldsymbol{\kappa})}. \tag{5.15}$$

where $z_{\boldsymbol{\kappa}} = \prod_{i \geq 1} i^{m_i} m_i!$, and $m_i = m_i(\boldsymbol{\kappa})$ is the number of parts of $\boldsymbol{\kappa}$ equal to i. Using this definition, Macdonald [59] proved that there are unique symmetric functions satisfying the following three properties:

1. *Orthogonality*: $\langle J_{\boldsymbol{\kappa}}, J_{\boldsymbol{\mu}} \rangle_{1/\lambda} = \delta_{\boldsymbol{\kappa},\boldsymbol{\mu}} j_{\boldsymbol{\kappa}}^{\lambda}$, where $j_{\boldsymbol{\kappa}}^{\lambda}$ is the normalization constant.

2. *Triangularity*: $J_{\boldsymbol{\kappa}} = \sum_{\boldsymbol{\mu}} v_{\boldsymbol{\kappa}\boldsymbol{\mu}} \Phi(\boldsymbol{\mu})$, where $v_{\boldsymbol{\kappa}\boldsymbol{\mu}} = 0$ unless $\boldsymbol{\kappa} \leq \boldsymbol{\mu}$.

3. *Normalization*: If $|\boldsymbol{\kappa}| = n$, then $v_{\boldsymbol{\kappa}\boldsymbol{\mu}} = n!$, where $\boldsymbol{\kappa} = (\underbrace{1, 1, \ldots, 1}_{n})$.

$J_{\boldsymbol{\kappa}}$ are, then, constructed by Gram-Schmidt orthogonalization relative to the scalar product on the ring of polynomials. Stanley [58] proved that the normalization constant is given by

$$j_{\boldsymbol{\kappa}}^{\lambda} = \prod_{s \in \boldsymbol{\kappa}} h_{\boldsymbol{\kappa}}^{\bullet}(s) h_{\bullet}^{\boldsymbol{\kappa}}(s). \tag{5.16}$$

In addition, Jack polynomials are eigenfunctions of the differential operator:

$$D(\lambda) = \frac{1}{2\lambda} \sum_{i=1}^{N} z_i^2 \frac{\partial^2}{\partial z_i^2} + \sum_{i \neq j} \frac{z_i^2}{z_i - z_j} \frac{\partial}{\partial z_i} \tag{5.17}$$

with the eigenvalues $e(\boldsymbol{\kappa})$:

$$e(\boldsymbol{\kappa}) = \frac{1}{\lambda} \sum_{i} \frac{\kappa_i(\kappa_i - 1)}{2} - \sum_{i} \frac{\kappa_i'(\kappa_i' - 1)}{2} + (N - 1)n \tag{5.18}$$

The operator (5.17) is closely related to the Hamiltonian (5.5).

There is another scalar product on which Jack polynomials are orthogonal:

$$\begin{aligned} (J_{\boldsymbol{\kappa}}, J_{\boldsymbol{\mu}})_{\lambda} &\equiv A_N^2 \left(\prod_{j=1}^{N} \int_0^L dx_j \right) \overline{J_{\boldsymbol{\kappa}}^{1/\lambda}(z_1, z_2, \ldots, z_N)} J_{\boldsymbol{\mu}}^{1/\lambda}(z_1, z_2, \ldots, z_N) \prod_{i<j} |z_i - z_j|^{2\lambda} \\ &= A_N^2 j_{\boldsymbol{\kappa}}^{\lambda} \prod_{s \in \boldsymbol{\kappa}} \frac{N + a'(s)/\lambda - l'(s)}{N + (a'(s) + 1)/\lambda - (l'(s) + 1)} \delta_{\boldsymbol{\kappa}, \boldsymbol{\mu}}. \end{aligned} \tag{5.19}$$

where $z_j = \exp(i2\pi x_j / L)$ and $A_N^2 = (1/L)^N \Gamma^N(1+\lambda)/\Gamma(1+\lambda N)$, and the bar over the polynomial denotes the complex conjugation. Note also that the multidimensional

integral above is equal to L^N times the constant term in

$$J_{\kappa}^{1/\lambda}(1/z_1, 1/z_2, \ldots, 1/z_N) J_{\mu}^{1/\lambda}(z_1, z_2, \ldots, z_N) \prod_{i \neq j} (1 - \frac{z_i}{z_j})^{\lambda}. \tag{5.20}$$

Eq. (5.19) has been proved by Macdonald [59] and also by Kadell [61].

Since Jack polynomials span the vector space of symmetric functions, they can be used to expand any symmetric functions. This property is particularly useful in calculating the correlation functions of the Calogero-Sutherland model as will be shown later. Here are some useful expansions[62, 63]:

$$\sum_{i=1}^{N} z_i^n = \frac{n}{\lambda} \sum_{\kappa, |\kappa|=n} \frac{[0']_{\kappa}^{\lambda}}{j_{\kappa}^{\lambda}} J_{\kappa}^{1/\lambda}(\{z_i\}), \tag{5.21}$$

$$\prod_{j=1}^{N} (1 - z_j)^a = \sum_{\kappa} \frac{\{-a\}_{\kappa}^{\lambda}}{\lambda^{|\kappa|} j_{\kappa}^{\lambda}} J_{\kappa}^{1/\lambda}(\{z_i\}), \tag{5.22}$$

where

$$[a]_{\kappa}^{\lambda} = \prod_{(i,j) \in \kappa} \{a + (j-1)/\lambda - (i-1)\} \tag{5.23}$$

$$\{a\}_{\kappa}^{\lambda} = \prod_{(i,j) \in \kappa} \{a - \lambda(i-1) + (j-1)\} \tag{5.24}$$

The sum in Eq. (5.22) extends over all possible partitions while in Eq. (5.21) it is restricted to partitions with *weight* $|\kappa| = n$. The prime in $[0']_{\kappa}^{\lambda}$ denotes that the product does not include the cell $(0, 0)$; otherwise the total product is trivially equal to zero. J_{κ} also satisfies

$$J_{\kappa}^{1/\lambda}(\{wz\}) = w^{|\kappa|} J_{\kappa}^{1/\lambda}(\{z\}). \tag{5.25}$$

since Jack polynomials are homogeneous functions of degree $|\boldsymbol{\kappa}|$.

5.2 Exclusion Statistics.

The notion of fractional exclusion statistics based on the so called "generalized Pauli exclusion principle" has first been formulated by Haldane and applied to the elementary topological excitations of general condensed matter systems [43]. This new concept of statistics is based on the structure of the single particle Hilbert space of the elementary excitations. More specifically, the change in the number of the available states (ΔD) in the Hilbert space as the number of particles (i.e., the elementary excitations) is changed (ΔN) for a given system with fixed boundary condition defines the statistics of the particles with the statistical parameter defined as $g = -\Delta D/\Delta N$. Hence, for example, the bosons and fermions are identified with $g = 0$ and $g = 1$, respectively.

To expose the exclusion statistics in the context of the Calogero-Sutherland model one introduces a pictorial representation of the eigenstates that make the identification of the excitation contents of the states easier [40]. Eq. (5.8) gives the occupation configurations of the pseudomomenta k_j for all the eigenstates of the Calogero-Sutherland model. The quantum numbers $\{I_j\}$ in Eq. (5.8) are distinct (half-odd) integers and

in the ground state are given by the following set

$$\{I_j^0\} = \left\{-\frac{N-1}{2}, -\frac{N-3}{2}, \ldots, \frac{N-3}{2}, \frac{N-1}{2}\right\}. \tag{5.26}$$

Therefore, the ground state pseudomomenta are given by

$$\{k_j^0\} = \left\{-\frac{\pi\lambda}{L}(N-1), -\frac{\pi\lambda}{L}(N-3), \ldots, \frac{\pi\lambda}{L}(N-3), \frac{\pi\lambda}{L}(N-1)\right\}. \tag{5.27}$$

The total ground state energy

$$E_N^0 = \sum_j (k_j^0)^2 = \pi^2\lambda^2 N(N^2-1)/3L^2 \tag{5.28}$$

The excited states are given by integer displacements of $\{I_j^0\}$. Therefore, two neighboring pseudomomenta for any arbitrary state must be separated by

$$\Delta k_j \equiv |k_j - k_{j-1}| = \frac{2\pi}{L}(\lambda - l), \tag{5.29}$$

where l is a non-negative integer.

In order to construct a picture that exposes the excitation content of the excited states, let λ be a rational number p/q with p and q coprimes and introduce a one-dimensional lattice with the lattice spacing equal to $2\pi/qL$. I assign each lattice point with 1 if that lattice point coincides with the value of one of the occupied pseudomomenta and with 0 if it does not. Hence, the ground state for $\lambda = 3/2$ and $N = 10$ is represented by $\ldots 0000000010010010010010010010010010000000\ldots$.

All the other excited states can be obtained from this ground state configuration by displacing the ones such that the number of zeroes between any pair of ones is equal to $p-1+ql$ where l is a non-negative integer.

Since $p-1$ zeroes are always required between the ones, they are called bound zeroes. The remaining zeroes are called unbound zeroes. The q consecutive unbound zeroes in the condensate of the pseudoparticles constitute a single hole excitation. Thus, if a pseudoparticle is removed from the ground state condensate, then there are p unbound zeroes in place where the one is removed. This state is forbidden if $q \neq 1$. In general a minimum of q ones must be removed so that they leave behind at least pq unbound zeroes which break up into p holes. From the view point of the particles (holes) the change in the number of available single particle states is p $(-q)$ while the change in the number of quasiparticles (quasiholes) in the system is $-q$ (p). Therefore, the statistical parameter g for the quasiparticle (quasihole) is $g = p/q = \lambda$ $(g = q/p = 1/\lambda)$. To summarize the fractional exclusion statistics, q particle excitations are accompanied by p hole excitations.

The configurations constructed above are representations of the diagrams of partitions $\mathcal{D}(\boldsymbol{\kappa})$ introduced in Sec. 5.1. The part κ_j corresponds to the displacement of jth quantum number from the ground state (i.e., $I_j - I_j^0$ if $I_1 > I_2 > \ldots > I_N$). The excitations given by $\boldsymbol{\kappa}$ include only the states with non-negative displacements (i.e.,

k_j moved only to the right) and all the other states are obtained by global translations. Therefore, each row (column) in the diagram corresponds to the particle (hole) excitations of the Calogero-Sutherland model.

Chapter 6

The Dynamical Current Correlation Functions of the Calogero-Sutherland Model.

Armed with the complete set of eigenfunctions, I will now calculate the dynamical polarization tensor of the Calogero-Sutherland model at zero temperature, namely

$$\Pi_{\mu\nu} = {}_N\langle j_\mu(r_1, t_1) j_\nu(r_2, t_2)\rangle_N \tag{6.1}$$

for $\mu, \nu = 0, 1$ with the density operator as the zeroth component of the generalized current

$$j_0(r, t) = \rho(r, t)$$

and the current operator as the other component:

$$j_1(r,t) = j(r,t)$$

and

$$\langle j_\mu(r_1,t_1) j_\nu(r_2,t_2)\rangle_N = \langle j_\mu(r_1) e^{-i(H_N^{GS} - E_N^{GS})(t_1-t_2)} j_\nu(r_2)\rangle_N \qquad (6.2)$$

(I will continue writing the subscript N for quantities that refer to N-particle system and omit the subscript in the thermodynamic limit.)

The full tensor will be shown to have the form:

$$\begin{pmatrix} \langle \rho(r,t)\rho(0,0)\rangle_N & \langle \rho(r,t) j(0,0)\rangle_N \\ \langle j(r,t)\rho(0,0)\rangle_N & \langle j(r,t) j(0,0)\rangle_N \end{pmatrix} = \int d\Omega F(\Omega) \begin{pmatrix} Q^2\cos(Qr) & \frac{iQE}{2m}\sin(Qr) \\ -\frac{iQE}{2m}\sin(Qr) & \left(\frac{E}{2m}\right)^2\cos(Qr) \end{pmatrix} \times \exp(-itE) \qquad (6.3)$$

Here the integration over the individual momenta of excitations is collectively denoted by Ω. E and Q are total energy and the total momentum of excitations, and $F(Q)$ is the formfactor. Their explicit form will be given in Sec. 6.2. The expression for the density-density correlation function, one of the components of the tensor is available [40]. I will show how to get the rest of the components.

The plan for this section is as follows: I will discuss the current operator and its expansion in Jack polynomials in Sec. 6.1, then I will compute the rest of the components of the polarizability tensor (6.3) in Sec. 6.2.

6.1 The Current Operator.

At low energies, when only quasiparticles with velocities around the Fermi points of the one-dimensional distribution are excited and have velocities equal to the sound velocity $v_s = \frac{\lambda \pi \rho_0}{m}$, the current is proportional to the density, $j \sim v_s \rho$.

At higher energies, when quasiparticles with different velocities are present, the current is no longer linearly proportional to the density.

Although the generalized exclusion principle (see Sec. 5.2) allows one to visualize all possible excitations, the operators of interest produce only some of all possible excitations. In particular, contributions to current correlation functions come from minimally excited wave functions, i.e. those that create the smallest number of excitations, maintaining charge neutrality.

To see the quasiparticle content of excitations produced by the current operator we examine its action on the ground state (5.2).

The density and current operators, as usual, are given by:

$$j(r) = \frac{1}{2m} \sum_{i}^{N} [p_i \delta(r - r_i) - \delta(r - r_i) p_i]$$

$$\rho(r) = \frac{1}{L} \sum_{i}^{N} \delta(r - r_i) - \frac{N}{L}$$

with $j_\mu(r,t) = \exp(iH_N^{CS}) j_\mu(r) \exp(-iH_N^{CS})$.

The idea of the calculation is very simple. First, I apply the current operator $j(r)$

to the ground state and observe that the action is equivalent to the multiplication by a symmetric function, representing the difference of normal and backflow.

Then, in order to see what kind of excitations this action produces, I expand the resulting expression in terms of eigenfuctions of the Hamiltonian (5.1), i.e products of a Jack polynomial (Sec. 5.1) and the ground state wavefunction (5.2). This allows me to follow the evolution of the system obtaining the value of the operator $\exp \imath H_N^{CS}(t_2 - t_1)$ on every excited state. Orthogonality of eigenfuctions further simplifies the resulting expression.

Before applying the current operator to the ground state, I shall rewrite the operator in a slightly different form. Expressing the periodic δ-function as an infinite series, I get:

$$j(r) = \frac{1}{2mL} \sum_{i=1}^{N} \left(\sum_{n=-\infty}^{\infty} \frac{\partial}{\partial x_i} e^{\frac{2\pi}{L} n(r - x_i)} + e^{\frac{2\pi}{L} n(r - x_i)} \frac{\partial}{\partial x_i} \right) \tag{6.4}$$

Changing variables as in Eq. (5.3), with $z = e^{\frac{2\pi}{L} r}$, I rewrite:

$$j(z) = \frac{\pi}{mL^2} \sum_{i=1}^{N} \left(\sum_{n=-\infty}^{\infty} -n z^n z_i^{-n} + n z^{-n} z_i^n + 2 z^n z_i^{-n+1} \frac{\partial}{\partial z_i} - 2 z^{-n} z_i^{n+1} \frac{\partial}{\partial z_i} \right) + 2 z_i \frac{\partial}{\partial z_i} \tag{6.5}$$

Now, the action on the ground state Eq. (5.2) produces:

$$j(z)\Psi_0 = \frac{\pi}{mL^2} \left[\sum_n -(n - \lambda(N-1)) z^n \left(\sum z_i^{-n} \right) + (n - \lambda(N-1)) z^{-n} \left(\sum z_i^n \right) \right.$$
$$\left. -2 z^n \lambda \sum_{i<j} \frac{z_i^{-n+1} - z_j^{-n+1}}{z_i - z_j} + 2 z^{-n} \lambda \sum_{i<j} \frac{z_i^{n+1} - z_j^{n+1}}{z_i - z_j} \right] \tag{6.6}$$

At this stage I have expressed the action of the current operator in terms of a function symmetric in z_i's. The next step, according to our strategy, is to express this symmetric function as eries in Jack polynomials. To facilitate this step I rewrite part of the second to last term in Eq. (6.6) introducing ξ_i:

$$\sum_{i<j} \frac{z_i^{-n+1} - z_j^{-n+1}}{z_i - z_j} = -\sum_{i<j} \frac{\xi_i^{n+1} - \xi_j^{n+1}}{\xi_i - \xi_j} + (N-1)\sum_i \xi_i^n \tag{6.7}$$

Therefore, collecting terms, I have the following expression for the current operator action on the ground state of the Calogero-Sutherland model:

$$\begin{aligned} j(z) = \frac{\pi}{mL^2}\sum_n \quad - \quad & z^n \left[(n - \lambda(N-1)) \left(\sum \xi_i^n \right) - 2\lambda \sum_{i<j} \frac{\xi_i^{n+1} - \xi_j^{n+1}}{\xi_i - \xi_j} \right] - \\ + \quad & \xi^n \left[(n - \lambda(N-1)) \left(\sum z_i^n \right) - 2\lambda \sum_{i<j} \frac{z_i^{n+1} - z_j^{n+1}}{z_i - z_j} \right] \end{aligned} \tag{6.8}$$

With this the expansion in Jack polynomials can be achieved as the expansion of the power series (the first term in square brackets) has been given in Eq. (5.21). The expression for the expansion of the second term in square brackets can be obtained by the action of the operator (5.17) on the power sums with the result:

$$\sum_{i<j} \frac{z_i^{n+1} - z_j^{n+1}}{z_i - z_j} = \frac{1}{\lambda} \sum_{\boldsymbol{\kappa}, =n} \frac{[0']^{\lambda}_{\boldsymbol{\kappa}}}{J^{\lambda}_{\boldsymbol{\kappa}}} \left[e(\boldsymbol{\kappa}) - \frac{n(n-1)}{2\lambda} \right] J^{1,\lambda}_{\boldsymbol{\kappa}}(\{z_i\}) \tag{6.9}$$

The notations used here have been introduced in Sec. 5.1, Eq.(5.23), (5.16), and (5.18).

Finally I obtain the expansion of the action of the current operator on the ground state of the Calogero-Sutherland model:

$$j(z) = \frac{\pi}{mL^2}\sum_n \quad -\frac{z^n}{\lambda}\sum_{\boldsymbol{\kappa}=n}\frac{[0']^\lambda_{\boldsymbol{\kappa}}}{j^\lambda_{\boldsymbol{\kappa}}}\left[2\lambda e(\boldsymbol{\kappa}) - n\lambda(N-1)+n\right]J^{1/\lambda}_{\boldsymbol{\kappa}}(\{\xi_i\}) + \\ +\frac{z^n}{\lambda}\sum_{\boldsymbol{\kappa}=n}\frac{[0']^\lambda_{\boldsymbol{\kappa}}}{j^\lambda_{\boldsymbol{\kappa}}}\left[2\lambda e(\boldsymbol{\kappa}) - n\lambda(N-1)+n\right]J^{1/\lambda}_{\boldsymbol{\kappa}}(\{z_i\}) \quad (6.10)$$

Inspection shows that $2\lambda e(\boldsymbol{\kappa}) - n\lambda(N-1)+n$ is proportional to the energy of the state $\boldsymbol{\kappa}$. $E_{\boldsymbol{\kappa}}$ given by the equation (5.6).

6.2 The Correlation Functions.

In this section I show that the dynamical current-current correlation function can be calculated exactly for the Calogero-Sutherland model using the expansions above and known properties of Jack polynomials.

Using the orthogonality relation Eq. (5.19) and its extension Eq. (5.20), I obtain the following expression for the current-current correlation function

$$N\langle 0|j(x,t)j(0,0)|0\rangle_N = \frac{1}{2(2\pi m\lambda)^2}\sum_{\boldsymbol{\kappa}}\frac{([0']^\lambda_{\boldsymbol{\kappa}})^2}{j^\lambda_{\boldsymbol{\kappa}}}\prod_{s(i,j)\in\boldsymbol{\kappa}}\frac{(N+(j-1)/\lambda-(i-1))}{(N+j/\lambda-i)} \\ \times E^2_{\boldsymbol{\kappa}}\cos(Qr)e^{-itE_{\boldsymbol{\kappa}}}. \quad (6.11)$$

where, as before,

$$E_{\boldsymbol{\kappa}} = (\frac{2\pi}{L})^2\sum_{i=1}^{N}(\kappa_i(\kappa_i-1) - \lambda\kappa'_i(\kappa'_i-1)+\lambda\kappa_i(N-1))$$

$$Q = \frac{2\pi}{L}\sum_{i=1}^{N}\kappa_i$$

In a totally analogous manner, the density-current correlation function is:

$$N\langle 0|\rho(x,t)j(0,0)|0\rangle_N = \frac{1}{2(2\pi m\lambda)^2}\sum_{\boldsymbol{\kappa}}\frac{([0']^{\lambda}_{\boldsymbol{\kappa}})^2}{j^{\lambda}_{\boldsymbol{\kappa}}}\prod_{s(i,j)\in\boldsymbol{\kappa}}\frac{(N+(j-1)/\lambda-(i-1))}{(N+j/\lambda-i)}$$

$$\times E_{\boldsymbol{\kappa}}Qi\sin(Qr)e^{-itE_{\boldsymbol{\kappa}}}. \qquad (6.12)$$

The correlation functions greatly simplify in the thermodynamic limit. The method I employ has been introduced in [46] and used intensively since then [40, 41, 42]. The method depends on the vanishing contribution from a large set of one-particle arrangements in the momentum space, i.e. possible partitions of a total momentum Q into a single particle κ_i's.

In general, for N particle system we consider partitions in no more that N parts, which assign single particle momenta to N particles. Therefore, the maximum length of any column in a partition is N. The length of a row (a single particle momentum) can, in principle, stretch out to infinity. Significantly, examination of the coefficients in the expansions of excitations in series of Jack polynomials shows, that $[0']^{\lambda}_{\boldsymbol{\kappa}}$ in Eq. (6.11) and (6.12) vanishes unless the diagram $D(\boldsymbol{\kappa})$ has no more than p columns of length longer than q and q rows of length longer than p. In other words, the intermediate states contributing to the dynamical current correlation functions has precisely p hole and q particle excitations. Only these (at most p) rows of unbounded

length and (at most q) columns of the length bounded by the number of particles survive in the thermodynamic limit.

Denoting the quasiparticle velocities x_i

$$x_i = \frac{\kappa_i}{N}$$

and quasihole's

$$y_j = \frac{\kappa'_j}{N}$$

the expressions (6.11) and (6.12) in the thermodynamic limit become:

$$\langle 0|j(r,t)j(0,0)|0\rangle = \frac{C}{(2m)^2}\prod_{i=1}^{q}\left(\int_0^\infty dx_i\right)\prod_{j=1}^{p}\left(\int_0^1 dy_j\right)F(q,p,\lambda|\{x_i,y_j\}) \times E^2\cos(Qr)e^{-iEt} \tag{6.13}$$

$$\langle 0|\rho(r,t)j(0,0)|0\rangle = \frac{C}{2m}\prod_{i=1}^{q}\left(\int_0^\infty dx_i\right)\prod_{j=1}^{p}\left(\int_0^1 dy_j\right)F(q,p,\lambda|\{x_i,y_j\}) \times QEi\sin(Qr)e^{-iEt} \tag{6.14}$$

where Q and E, the total momentum and energy, are given in units of $\hbar$ and $\hbar^2/2m$ by

$$Q = 2\pi\rho_0\left(\sum_{j=1}^{q}x_j - \sum_{j=1}^{p}y_j\right). \tag{6.15}$$

$$E = (2\pi\rho_0)^2\left(\sum_{j=1}^{q}\epsilon_P(x_j) + \sum_{j=1}^{p}\epsilon_H(y_j)\right). \tag{6.16}$$

with $\rho_0 = N/L$, $\epsilon_P(x) = x(x+\lambda)$ and $\epsilon_H(y) = \lambda y(1-y)$. $x_j(\epsilon_P)$ and $y_j(\epsilon_H)$ are normalized momentum (energy) of the quasiparticles and the quasiholes, respectively.

The normalization constant C is given by

$$C = \frac{\lambda^{2p(q-1)}\Gamma^2(p)}{2\pi^2 p!q!}\frac{\Gamma^q(\lambda)\Gamma^p(1/\lambda)}{\prod_{i=1}^{q}\Gamma^2(p-\lambda(i-1))\prod_{j=1}^{p}\Gamma^2(q-(j-1)/\lambda)} \prod_{j=1}^{p}\left(\frac{\Gamma(q-(j-1)/\lambda)}{\Gamma(1-(j-1)/\lambda)}\right)^2 \tag{6.17}$$

Finally, the form factor $F(q,p,\lambda|\{x_i,y_j\})$ is given by

$$F(m,n,\lambda|\{x_i,y_j\}) = \prod_{i=1}^{m}\prod_{j=1}^{n}(x_i+\lambda y_j)^{-2}\frac{\left(\prod_{i<j}(x_i-x_j)^2\right)^{\lambda}\left(\prod_{i<j}(y_i-y_j)^2\right)^{1/\lambda}}{\prod_{i=1}^{m}\epsilon_P(x_i)^{1-\lambda}\prod_{j=1}^{n}\epsilon_H(y_j)^{1-1/\lambda}}. \tag{6.18}$$

6.3 The Static Limit and Conservation Laws.

Since a density perturbation does not create any instantaneous current, in the static limit the off-diagonal elements of the polarization tensor vanish. The current density mapping, derived by Shastry *et. al.* [35], gives a simple relationship between the diagonal elements in the static limit.

$$\langle 0|j(r)j(0)|0\rangle = -\frac{\lambda}{2m^2r^2}\langle 0|\rho(r)\rho(0)|0\rangle$$

This implies an identity between two quite involved integrals, namely: the static limit of (6.13) and the static limit of the density-density correlation function.

The continuity relation

$$\frac{\partial^2}{\partial t_1\partial t_2}\langle 0|\rho(r_1,t_1)\rho(r_2,t_2)|0\rangle = \frac{\partial^2}{\partial r_1\partial r_2}\langle 0|j(r_1,t_1)j(r_2,t_2)|0\rangle$$

can be directly seen to be trivially satisfied.

As a last check, I verify that the polarizability tensor is transverse, for instance:

$$\frac{\partial}{\partial t_2}\langle 0|\rho(r_1,t_1)\rho(r_2,t_2)|0\rangle = -\frac{\partial}{\partial t_1}\langle 0|\rho(r_1,t_1)j(r_2,t_2)|0\rangle$$

6.4 Discussion.

Extensions Calogero-Sutherland model has proved very fruitful in elucidating the structure of integrable one-dimensional models. In particular, Haldane and Shastry [50] have independently discovered the integrability of the SU(2) spin model on a lattice with the inverse square interaction (often called Haldane-Shastry chain) . The dynamical version of this model has been shown to possess a Yangian symmetry [49].

D. Uglov exploited the Yangian symmetry to construct the the complete basis of eigenstates of the dynamical Haldane-Shastry model which turn out to be a generalization of Jack polynomials. The method of Jack polynomials has been applied to the calculation of the correlation functions of this model as well [52].

This somewhat fortunate situation when the symmetry of the Hamiltonian allows the constrction of a complete orthogonal basis of eigenstates has yet to be replicated for the dynamical Haldane-Shastry model in a magnetic field. And, more ambitiously, perhaps the infinite symmetry of the Hamiltonian describing two-dimensional elec-

trons in a magnetic field [53, 54] can be exploited to provide a further insight to the Quantum Hall effect.

Part III

Appendices.

Appendix A

Density Operator Projected on the N^{th} Landau Level.

Below I display the explicit form of the remaining dynamical variable (after the lower Landau level electrons have been integrated out to give the dielectric constant (3.10)). This is the projected density operator, which appears in the Hamiltonian (3.9).

$$\rho(\mathbf{q}) = \int dxdy \sum_{X,X'} \Psi^{\dagger}_{X} \Psi_{X'} e^{-i\mathbf{q}\mathbf{r}} a^{\dagger}_{X} a_{X'} =$$

$$= \frac{1}{\pi^{1/2} 2^{N} N! \ell} \int dx \sum_{X,X'} e^{-iq_x x - \frac{(x-X')^2}{2\ell^2} - \frac{(x-X)^2}{2\ell^2}} \times$$

$$H_N\left(\frac{x-X'}{\ell}\right) H_N\left(\frac{x-X}{\ell}\right) \delta\left(X - X' - q_y \ell^2\right) a^{\dagger}_{X} a_{X'}$$

Summing over X' and changing the variable to $u = (x - X)/\ell$ we proceed:

$$\begin{aligned}
\rho(\mathbf{q}) &= \sum_X \frac{e^{-iq_x X}}{\pi^{1/2} 2^N N!} \int du e^{-(u+iq_x\ell/2)^2} e^{-(q\ell/2)^2} \times \\
&\quad H_N\left(u - \frac{q_y\ell}{2}\right) H_N\left(u + \frac{q_y\ell}{2}\right) a^\dagger_{X-q_y\ell^2/2} a_{X-q_y\ell^2/2} = \\
&= \sum_X \frac{e^{-iq_x X-(q\ell/2)^2}}{\pi^{1/2} 2^N N!} \int dv e^{-v^2} H_N\left(v - \frac{iq_x + q_y}{2}\ell\right) \times \\
&\quad H_N\left(v - \frac{iq_x - q_y}{2}\ell\right) a^\dagger_{X-q_y\ell^2/2} a_{X-q_y\ell^2/2} \\
&= \sum_X e^{-iq_x X} e^{-(q\ell/2)^2} L_N\left(\frac{q^2\ell^2}{2}\right) a^\dagger_{X-q_y\ell^2/2} a_{X-q_y\ell^2/2}. \qquad \text{(A.1)}
\end{aligned}$$

where in the third and fourth line I have shifted the variable of integration $v = u - iq_x\ell/2$ to obtain the standard integral[74] in the last line.

It is important that the density operator is modulated by $F(q) \equiv e^{-(q\ell/2)^2} L_N\left(\frac{q^2\ell^2}{2}\right)$, due to oscillatory nature of electronic wavefunctions on higher Landau levels. $F(q)$ is often referred to as the form-factor.

Appendix B

Hartree-Fock Decoupling.

Following the logic of Hartree-Fock decoupling of [29], one writes:

$$\frac{1}{2L_xL_y}\sum_{\mathbf{q}}\tilde{u}(\mathbf{q})\rho(\mathbf{q})\rho(-\mathbf{q}) \rightarrow$$
$$\frac{n_L}{2}\sum_{\mathbf{q}}\tilde{u}(\mathbf{q})F^2(q)\sum_{X}e^{-iq_xX}a^{\dagger}_{X_-}a_{X_-}\frac{2\pi\ell^2}{L_xL_y}\sum_{X'}e^{-iq_xX'}\langle a^{\dagger}_{X'_-}a_{X'_-}\rangle$$
$$-\frac{1}{2L_xL_y}\sum_{\mathbf{q}}\sum_{X,X'}\tilde{u}(\mathbf{q})F^2(q)e^{-iq_x(X-X')}a^{\dagger}_{X_-}a_{X'_-}\langle a^{\dagger}_{X'_-}a_{X_-}\rangle$$

In the direct term one easily recognizes the order parameter. The exchange term is evaluated using:

$$\langle a^{\dagger}_{X_-}a_{X_-}\rangle = \sum_{\kappa}\Delta(\kappa)e^{i\kappa_xX}\delta(q_y-\kappa_y).$$

which can be obtained by inverting the definition of $\Delta(\mathbf{q})$. The nonzero terms in the sum are those X' where $X' = X + \kappa_y\ell^2$. That creates the term $a^{\dagger}_{X-\kappa_y\ell^2/2}a_{X-3\kappa_y\ell^2/2}$

that is brought to the standard from by the shift in X, $\tilde{X} = X + \kappa_y \ell^2$.

$$-\frac{1}{2L_x L_y}\sum_{\kappa}\Delta(\kappa)\sum_{X} a^{\dagger}_{X+\kappa_y\ell^2/2}a_{X-3\kappa_y\ell^2/2}e^{i\kappa_x X}\sum_{\mathbf{q}}\tilde{u}(\mathbf{q})F^2(q)e^{i\ell^2 q_x\kappa_y} =$$

$$= -\frac{1}{2L_x L_y}\sum_{\kappa}\Delta(\kappa)\sum_{\tilde{X}} e^{i\kappa_x\tilde{X}}a^{\dagger}_{\tilde{X}-}a_{\tilde{X}-}\sum_{\mathbf{q}}\tilde{u}(\mathbf{q})F^2(q)e^{i\ell^2(q_x\kappa_y - q_y\kappa_x)} =$$

$$= -\sum_{\kappa}\Delta(\kappa)\sum_{\tilde{X}} e^{i\kappa_x\tilde{X}}a^{\dagger}_{\tilde{X}-}a_{\tilde{X}-}\int\frac{d^2q}{(2\pi)^2}\tilde{u}(\mathbf{q})F^2(q)e^{i\ell^2(q_x\kappa_y - q_y\kappa_x}$$

Appendix C

Integrals.

Recall. that the order parameter in Sec. 3.6.1 and 4.3 is periodic $\Delta(x') = \Delta(x' + \Lambda)$ and:

$$\Delta(x') = \Theta(\frac{\Lambda}{4} - |x'|)$$

and the effective interaction can be written in the form:

$$u_{HF}^{eff}(x - x') = u_0\Theta(2R_c - |x - x'|)f(|x - x'|)$$

with

$$f(|x - x'|) = \begin{cases} 1. & \text{for uniform density in the } \hat{y} \text{ direction} \\ J_0(Q\sqrt{4R_c^2 - |x - x'|}). & \text{for density modulated in the } \hat{y} \text{ direction.} \end{cases}$$

Calculating the cohesive energy in Eq. (3.22), Eq. (4.4), and Eq. (4.31) one encounters the integrals of the following form:

$$I = \int dx dx' \Theta(2R_c - |x - x'|)\Theta(\frac{\Lambda}{4} - |x|)\Theta(\frac{\Lambda}{4} - |x'|) f(|x - x'|)$$

I will show that this integral can be simplified. (The condition $\frac{\Lambda}{4} < 2R_c$ is assumed to hold.) The integrand is nonzero if either of the following two conditions is satisfied:

$$\begin{cases} x' < x \\ x' > \frac{\Lambda}{2} - 2R_c, \text{ or} \end{cases}$$

$$\begin{cases} x' > x \\ x' < \frac{\Lambda}{2} + 2R_c \end{cases}$$

The resulting region of integration is shown on the graph C.1. The integral is then:

$$I = \int_{-\frac{\Lambda}{4}}^{\frac{\Lambda}{4}} dx \int_{-\frac{\Lambda}{4}}^{\frac{\Lambda}{4}} dx' f(|x - x'|) + \int_{-\frac{\Lambda}{4}}^{\frac{3\Lambda}{4} - 2R_c} dx \int_{x - 2R_c}^{-\frac{\Lambda}{4}} dx' f(|x - x'|) +$$
$$+ \int_{\frac{3\Lambda}{4} - 2R_c}^{\frac{\Lambda}{4}} dx \int_{\frac{3\Lambda}{4}}^{x + 2R_c} dx' f(|x - x'|) =$$
$$= \int_{-\frac{\Lambda}{4}}^{\frac{\Lambda}{4}} dx \int_{-\frac{\Lambda}{4}}^{\frac{\Lambda}{4}} dx' f(|x - x'|) + 2 \int_{\frac{3\Lambda}{4} - 2R_c}^{\frac{\Lambda}{4}} dx \int_{\frac{3\Lambda}{4}}^{x + 2R_c} dx' f(|x - x'|)$$

One can take advantage of the fact the integrand is the function of $|x - x'|$ only by changing variables:

$$u = x' - x$$

$$v = x' + x$$

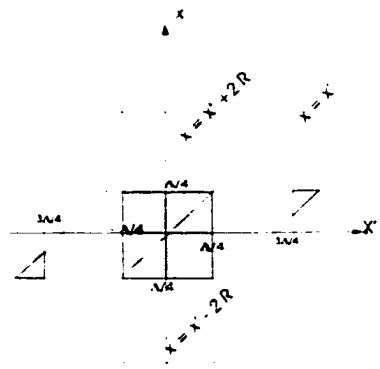

Figure C.1: Integration region (shown in gray) for the calculation of the cohesive energy.

The Jacobian of this transformation is equal to 2. As an illustration, the resulting triangular integration region in the new coordinates is shown on the Figure C.2. In the new coordinates the integral over v can be done and the final expression for the integral is:

$$I = \int_0^{\frac{\Lambda}{2}} du(\Lambda - 2u) f(|u|) + \int_{\frac{\Lambda}{2}}^{2R_c} du(2u - \Lambda) f(|u|) = \tag{C.1}$$

$$= 2\int_{\frac{\Lambda}{2}}^{2R_c} du\, u f(|u|) - 2\int_0^{\frac{\Lambda}{2}} du\, u f(|u|) - \Lambda \int_0^{2R_c} du f(|u|) + 2\Lambda \int_0^{\frac{\Lambda}{2}} du f(|u|)$$

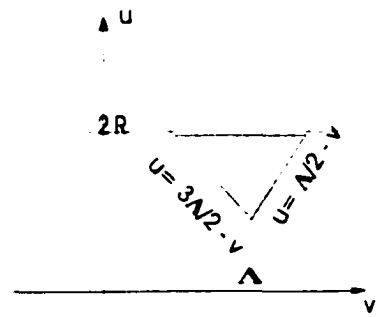

Figure C.2: Triangular integration region (shown in gray) in the new coordinates.

Appendix D

Small Wavevector Limit of the Cohesive Energy in the Parallel Alignment.

Recall. that the order parameter of the stripe modulated in the $\hat{y}$ direction has the form:

$$\Delta(x.y) = \Theta(\frac{\lambda}{4} - |x|)\{1 - \xi\frac{\sin(Q_y L_y)}{Q_y L_y} + \xi\cos(Q_y y)\}$$

as we saw in Eq. (4.29). corresponding to the stripe that consists of a uniform and modulated parts.

My objective here is to use this order parameter that has the correct limit at

$Q_y \to 0$ and perform the same calculation of the cohesive energy as in Sec. 4.3. The total cohesive energy is made up of three pieces:

- interstripe interaction

$$\int dxdy \int dx'dy' \Delta(x,y) u_{eff}^{HF}(x-x', y-y') \Delta(x',y').$$

- the energy of the uniform state that we subtract

$$\bar{\nu} \int dxdx' \Theta(2R_c - |x-x'|) + \frac{v}{2} \frac{\sin Q_y L_y}{Q_y L_y} = R_c + \frac{v}{2} \frac{\sin Q_y L_y}{Q_y L_y}.$$

- and the external potential energy.

The external potential energy contribution is evaluated similarly to (4.33):

$$\begin{aligned}
&\frac{1}{2\bar{\nu}} \int dxdy v \cos(Q_y y) \Theta(\frac{\lambda}{4} - |x|)(1 - \xi \frac{\sin(Q_y L_y)}{Q_y L_y} + \xi \cos(Q_y y) = \\
&= \frac{v}{2\bar{\nu}} \int dx \Theta(\frac{\lambda}{4} - |x|) \int dy \{1 - \xi \frac{\sin(Q_y L_y)}{Q_y L_y} + \xi \cos(Q_y y)\} \cos(Q_y y) = \\
&= \frac{v}{2} \left\{ \left(1 - \xi \frac{\sin Q_y L_y}{Q_y L_y}\right) \frac{\sin Q_y L_y}{Q_y L_y} + \frac{\xi}{2} \left(1 + \frac{\sin 2Q_y L_y}{2Q_y L_y}\right) \right\} \equiv \\
&\equiv \frac{v}{2} \frac{\sin Q_y L_y}{Q_y L_y} + \xi \Gamma.
\end{aligned}$$

where I have introduced the notation:

$$\Gamma = \frac{v}{2} \left\{ \frac{1}{2} \left(1 + \frac{\sin 2Q_y L_y}{2Q_y L_y}\right) - \left(\frac{\sin Q_y L_y}{Q_y L_y}\right)^2 \right\}$$

I would like to remark that $\Gamma \to 0$ as $Q_y \to 0$.

Calculation of the interstripe interaction term gives the following result:

$$\left(1-\xi\frac{\sin Q_y L_y}{Q_y L_y}\right)^2 E + 2\xi\left(1-\xi\frac{\sin Q_y L_y}{Q_y L_y}\right)\frac{\sin Q_y L_y}{Q_y L_y} J + \frac{\xi^2}{2}\left(1+\frac{\sin 2Q_y L_y}{2Q_y L_y}\right) J. \tag{D.1}$$

where I have introduced the notation for the energy of the uniform part

$$E = \frac{1}{\lambda}\left[\frac{\lambda^2}{2} - 2\lambda R_c - 4R_c^2\right]$$

and that of the modulated part

$$J = \left[4\sqrt{4R_c^2-\frac{\lambda^2}{4}}J_1\left(Q_y\sqrt{4R_c^2-\frac{\lambda^2}{4}}\right) - \right.$$
$$\left. -4R_c J_1(2Q_y R_c) - \lambda\sin(2Q_y R_c) + 2\lambda Q_y\int_0^{\lambda/2} du J_0(Q_y\sqrt{4R_c^2-u^2})\right] / Q_y\lambda$$

Notice that since $J_1(z)\sim z/2$ and $J_0(z)\sim 1$, as $Q_y\to 0$ the energy of the modulated part J goes over to E as it should. Obviously in the limit of very long wavelength the cost energy a modulated stripe is reduced to the energy of the uniform one. The total interaction energy (D.1) is reduced to just the energy of one totally uniform stripe.

The minimal value of ξ is calculated by minimizing the interaction and external potential terms:

$$\xi_{min} = -\frac{V + 2\frac{\sin Q_y L_y}{Q_y L_y}(J-E)}{J\left(1+\frac{\sin Q_y L_y}{Q_y L_y}\right) + 2E\left(\frac{\sin Q_y L_y}{Q_y L_y}\right)^2 - 4J\left(\frac{\sin Q_y L_y}{Q_y L_y}\right)^2}$$

The minimal value of the total cohesive energy is then:

$$\epsilon = \epsilon_0 - \frac{\left(V + 2\frac{\sin Q_y L_y}{Q_y L_y}(J - E)\right)^2}{2\left\{J\left(1 + \frac{\sin Q_y L_y}{Q_y L_y}\right) + 2E\left(\frac{\sin Q_y L_y}{Q_y L_y}\right)^2 - 4J\left(\frac{\sin Q_y L_y}{Q_y L_y}\right)^2\right\}}$$

Finally, in the limit $Q_y R_c \ll Q_y L_y \ll 1$ the cohesive energy goes to:

$$\epsilon = \epsilon_0 - \frac{2v^2}{3\epsilon_0}(Q_y L_y)^2$$

Part IV

Bibliography.

Bibliography

[1] L. Landau. *Zs. Phys.* **64**. 629 (1930):

[2] D. Langbein. *Phys. Rev.* **180**. 633 (1969):

[3] D. R. Hofstadter. *Phys. Rev. B* **14**. 2239 (1976):

[4] C. Zhang and R. R. Gerhardts. *Phys. Rev. B* **41**. 12850 (1990):

[5] D. C. Tsui. H. L. Stormer. and A.C. Gossard. *Phys. Rev. Lett.* **48**. 1559 (1982):

[6] J. P. Eisenstein. M.P. Lilly. K.B. Cooper. L.N. Pfeiffer. K.W. West in *The Proceedings of the 11th International Winterschool on New Developments in Solid State Physics*. Mauterndorf. Austria. February. 2000:

[7] H. L. Stormer *Bull. Am. Phys. Soc* **38**. 235 (1993):

[8] M.P. Lilly. K. B. Copper. J. P. Eisenstein. L. N. Pfeiffer. and K. W. West. *Phys. Rev. Lett.* **82**. 394 (1999):

[9] M.P. Lilly, K. B. Copper, J. P. Eisenstein, *Phys. Rev. Lett.* **83**, 824 (1999);

[10] R. R. Du, D. C. Tsui, H. L. Stormer, L. N. Pfeiffer, K. W. Baldwin, and K. W. West, *Solid State Comm.* **109**, 389 (1999);

[11] M.M. Fogler, A.A. Koulakov, and B.I. Shklovskii, *Phys. Rev. B* **54**, 1853 (1996);

[12] M. M. Fogler, cond-mat/0111001;

[13] R. Moessner and J. T. Chalker, *Phys. Rev. B* **54**, 5006 (1996);

[14] I. L. Aleiner and L. I. Glazman, *Phys. Rev. B* **52** , 11296 (1995);

[15] T. Ando and Y. Yemura, *J. Phys. Soc. Japan* **37**, 1044 (1974);

[16] A. H. MacDonald and Matthew P. A. Fisher, *Phys. Rev. B* **61**, 5724 (2000);

[17] E. H. Rezavi, F. D. M. Haldane, K. Yang, *Phys. Rev. Lett.* **83**, 1219 (1999);

[18] R. Côté and H.A. Fertig, *Phys. Rev. B* **62**, 1993 (2000);

[19] Anna Lopatnikova, Steven H. Simon, Bertran I. Halperin, and X.-G. Wen, *Phys. Rev. B* **64**, 155301 (2001);

[20] A. H. Macdonald and D.B Murray, *Phys. Rev. B* **32**, 2291 (1985);

[21] A. Kol and N. Read, *Phys. Rev. B* **48**, 8890 (1993);

[22] S.-J. Yang, Y. Yue, and Z.-B. Sue, cond-mat/0006009;

[23] A. Endo and Y. Iye, *Solid State Comm.* **117**, 249 (2001);

[24] D. Weiss, K. von Klitzig, K. Ploog, G. Weimann, *Europhys. Lett.* **8**, 179 (1989);

[25] T. Aoyama, K. Ishikawa, and N. Maeda, cond-mat/0106484 ;

[26] K. B. Copper, M.P. Lilly, J. P. Eisenstein, T. Jungwirth, L. N. Pfeiffer, and K. W. West, cond-mat/0104243 ;

[27] D. Yoshioka, cond-mat/0106618;

[28] D. N. Sheng, Z. Wang, and B. Friedman, cond-mat/0112233;

[29] H. Fukuyama, P.M. Platzman, and P.W. Anderson, *Phys. Rev. B* **19**, 5211 (1979);

[30] F. Stern, *Phys. Rev. Lett.* **18**, 546 (1967);

[31] J. Moser, *Adv. Math.* **16**, 197 (1975);

[32] F. Calogero, *J. Math. Phys.* **10**,2191 (1969); B. Sutherland, *Phys. Rev.* **A4**, 2019 (1971);

[33] B. Sutherland, in *Lecture Notes in Physics* **242**, Springer-Verlag, 1985;

[34] B. Simons, P.A. Lee, and B. L. Altshuler, *Phys. Rev. Lett.* **70**, 4122 (1993);

[35] N. Taniguchi, B. S. Shastry, B. L. Altshuler, *Phys. Rev. Lett.* **75**, 3724 (1995);

[36] R. B. Laughlin, *Phys. Rev. Lett.* **50**, 1395 (1983);

[37] X. G. Wen, *Phys. Rev. Lett.* **64**, 216 (1990), *Phys. Rev. B* **41**, 12838 (1990); *Mod. Phys. Lett. B* **5**, 39 (1991);

[38] A. P. Polychronakos, Phys. Rev. Lett. **69**, 703 (1992);

[39] F. D. M. Haldane, in the *Proceedings of the 16th Taniguchi Symposium*, Kashikijima, Japan, October 26-29, 1993, eds. A. Okiji and N. Kawakami, Springer-Verlag, 1994;

[40] Z. N. C. Ha, *Phys. Rev. Lett.* **73**, 1574 (1994), *Nuclear Physics* **435**, 604 (1995);

[41] F. Lesage, V. Pasquier, D. Serban, *Nuclear Physics* **435**, 585 (1995);

[42] D. Serban, F. Lesage, V. Pasquier, *Nuclear Physics* **466**, 499 (1996);

[43] F. D. M. Handane, *Phys. Rev. Lett.* **66**, 1529 (1991);

[44] N. Kawakami, *Phys. Rev. B* **46**, 1005 (1992); and **46**, 3192 (1992);

[45] F. D. M. Haldane and M. R. Zirnbauer, *Phys. Rev. Lett.* **71**, 4055 (1993);

[46] P. J. Forrester, *Phys. Lett. A* **179**, 127 (1993); *Nucl. Phys. B* **388**, 671 (1992);

[47] L.S. Tevlin and J.L. Birman, *Phys. Lett. A* **227**, 387 (1997);

[48] M. Stone, *Int. J. of Mod. Phys. bf B 5*; and *Phys. Rev. B* **45**, 14 156 (1992);

[49] D. Bernard, M. Gaudin, F.D.M. Haldane, and V. Pasquier, *J. of Phys.* **A 26**, 5219 (1993);

[50] B.S. Shastry *Phys. Rev. Lett.* **60**, 639 (1988), F.D.M. Haldane *Phys. Rev. Lett.* **60**, 635 (1988);

[51] D. Uglov in *Calogero-Moser-Sutherland Models*, eds J.-F. van Diej and L. Vinet, Springer, 2000;

[52] T. Yamamoto and M. Arikawa, *J. Phys.* **A 32**, 3341 (1999).

[53] S. Iso, D. Karabali, and B. Sakita *Nuclear Physics* **388**, 700 (1992); D. Karabali *Nuclear Physics* **428**, 531 (1994);

[54] A. Capelli, C. Trugenberger, and G. Zemba, *Nuclear Physics* **396**, 465 (1993);

[55] J. Kaneko, *SIAM J. Math. Anal.* **24**, 1086 (1993); K. W. J. Kadell, *Compos. Math.* **87**, 5 (1993) ;

[56] P. J. Forrester, *Nucl. Phys.* **B416**, 377 (1994);

[57] H. Jack. *Proc. Roy. Soc. Edinburgh Sect. A* **69**. 1 (1969-1970):

[58] R. P. Stanley. *Adv. Math.* **77**. 76 (1989):

[59] I. G. Macdonald. *Symmetric Functions and Hall Polynomials*. Oxford Univ. Press. Oxford. 1995:

[60] I. G. Macdonald. *Lecture Notes in Math.* **1271**. 189 (1987).

[61] K. W. J. Kadell. *Compos. Math.* **87**. 5 (1993):

[62] P. J. Hanlon. R. P. Stanley. and J. R. Stembridge. *Contemp. Math.* **138**. 151 (1992):

[63] Z. Yan. *Contemp. Math.* **138**. 239 (1992):

[64] Umberto Eco. *Kant and Platypus*. Harcout Brace & Company. 1997:

[65] *Newsweek*. 16 December 1957:

[66] L. D. Landau and E. M. Lifshitz. *Mechanics* (Butterworth-Heinemann. 1976):

[67] L. D. Landau and E. M. Lifshitz. *The Classical Theory of Fields* (Butterworth-Heinemann. 1997):

[68] L. D. Landau and E. M. Lifshitz. *Quantum Mechanics* (Butterworth-Heinemann. 1997):

[69] Steven M. Girvin. *The Quantum Hall Effect: Novel and Broken Symmetries* in *Topological Aspects of Low Dimensional Systems* (Les Houches. Summer School) edited by A. Comtet. T. Jolicoeur . S. Ouvry. and F. David (Springer Verlag. 2000):

[70] *The Quantum Hall Effect. 2nd Ed.*. edited by Richard E. Prange and Steven M. Girvin (Springer-Verlag. New York. 1990):

[71] *Perspectives in Quantum Hall Effects*. eds. S. Das Sarma and A. Pinczuk. (John Wiley. New York. 1997):

[72] G. Baym and C. Pethick. *Landau Fermi-liquid theory: Concepts and Applications*. (John Wiley. New York. 1992):

[73] M. L. Mehta *Random Matrices*. (Academic Press. 1991):

[74] I.S. Gradshtein and I.M. Ryzhik. *Tables of Integrals. Series. and Products* (Academic Press. 1994):